1 Title:

2 DNA-PK controls cyclic dinucleotide-associated type I Interferon responses

3 Authors:

- 4 Clara Taffoni¹, Isabelle K. Vila¹, Jane Jardine², Moritz Schussler¹, Joe McKellar¹, Morgane
- 5 Chemarin¹, Joanna Re¹, Yasmine Messaout-Nacer¹, Insaf El Mansouri¹, George P Chrousos³,
- 6 Nicolas Bidère², Karim Majzoub¹, Dimitrios Vlachakis^{3,4,5,*}, Nadine Laguette^{1,*}

7 Affiliations:

- 8 ¹ IGMM, université de Montpellier, CNRS UMR5535, Montpellier, France
- ⁹ Team SOAP, CRCI2NA, Nantes Université, Inserm, CNRS, Université d'Angers Nantes
- 10 France, Equipe Labellisée Ligue Contre le Cancer Paris France
- 11 ³ Laboratory of Genetics, Department of Biotechnology, School of Applied Biology and
- Biotechnology, Agricultural University of Athens, 75 Iera Odos, 11855 Athens, Greece
- ⁴ University Research Institute of Maternal and Child Health & Precision Medicine, and
- 14 UNESCO Chair on Adolescent Health Care, National and Kapodistrian University of Athens,
- 15 "Aghia Sophia" Children's Hospital, 11527 Athens, Greece
- ⁵ School of Informatics, Faculty of Natural & Mathematical Sciences, King's College London,
- WC2R 2LS, Bush House, Strand, London, U.K.
- *Correspondance to:

- Nadine Laguette: nadine.laguette@cnrs.fr; nadine.laguette@igmm.cnrs.fr; and Dimitrios
- Vlachakis : dimitris@aua.gr

Summary (200words):

22

23

24

25

26

27

28

29

30

31

32

33

34

35

36

37

38

39

40

41

42

43

44

45

46

47

48

49

50

51

52

Cytosolic dsDNAs are potent immune-stimulatory molecules that trigger inflammation in several human pathologies ^{1,2}. A major pathway for the detection of cytosolic dsDNA relies on the cyclic GMP-AMP (cGAMP) synthase (cGAS) that produces the 2'3'-cGAMP cyclic dinucleotide (CDN) for activation of the Stimulator of Interferon Genes (STING) adaptor protein that subsequently drives type I Interferon (IFN) responses ^{3,4}. Here, we investigated the mechanism regulating intracellular 2'3'-cGAMP levels. We show that the DNA-dependent protein kinase catalytic subunit (DNA-PKcs), a major player in the repair of double-strand breaks, directly regulates intracellular levels of 2'3'-cGAMP, thereby reducing STING activation. We describe that the binding of 2'3'-cGAMP to DNA-PKcs occurs in its catalytic cleft, impeding its kinase function. Contrary to other CDN regulatory mechanisms that have been shown to primarily regulate extracellular 2'3'-cGAMP, we show that DNA-PKcs also interacts with the 3'3'-cGAMP bacterial CDN, limiting its capacity to activate STING signaling. Furthermore, we found that DNA-PKcs decreases the potency of pharmacological STING activators. As STING is a major target for therapeutic interventions aiming to boost inflammatory responses in immunosuppressed contexts ⁵, our data bear important implications for drug development and deepens our understanding of inflammatory regulation in response to CDNs.

Main text:

The presence of DNA in the cytosol is sensed as a danger signal and promotes the activation of inflammatory responses ⁶. A major pathway involved in the detection of cytosolic dsDNA relies on the cyclic GMP-AMP (cGAMP) synthase (cGAS) ⁷ that catalyzes the production of the 2'3'-cGAMP cyclic dinucleotide (CDN), which in turn binds and activates the Stimulator of Interferon Genes (STING) adaptor protein ⁸. The interaction of 2'3'-cGAMP with STING drives the assembly of a signalosome where the Tank Binding Kinase 1 (TBK1) catalyzes phosphorylation-dependent activation of transcription factors, such as the Interferon Regulatory Factor 3 (IRF3), that drive the expression of inflammatory cytokines and type I Interferons (IFNs) ^{9,10}. Activation of the cGAS-cGAMP-STING signaling axis is essential in response to pathogen infection, cellular stress, or tissue damage which are contexts where immune stimulatory dsDNAs are exposed in the cytosol. However, chronic activation of this signaling pathway is reported in several human pathologies, such as auto-inflammatory diseases or

- cancer, where it is responsible for chronic low-grade disease-promoting inflammation, leading
- to immune dysfunction and tissue damage ⁶.
- To mitigate the deleterious effects of unwanted activation of the cGAS-cGAMP-STING
- 56 pathway, several regulatory layers have been described to control directly cGAS and/or STING
- 57 activation ^{11,12}. In contrast, few direct regulators of the 2'3'-cGAMP molecule have been
- documented in mammals ¹³⁻¹⁵, all of which expected to act on extracellular 2'3'-cGAMP. This
- is striking since 2'3'-cGAMP is an essential component of the cGAS-STING axis involved
- 60 notably in signal amplification and propagation ¹⁶. Additionally, despite several CDNs of
- bacterial origins shown to be active in mammalian cells ^{17,18}, no mechanism ensuring their
- regulation has been described to date. Here, we unveil the DNA-PK catalytic subunit (DNA-
- 63 PKcs) of the DNA-PK complex, canonically involved in double-strand break repair, as an
- 64 intracellular regulator of CDNs.

DNA-PK regulates 2'3-cGAMP-associated STING signaling

- 66 DNA-PK has been shown to play dichotomous roles in the regulation of STING-dependent
- 67 inflammatory responses. Specifically, DNA-PK can operate as an alternative cytosolic dsDNA
- detection pathway capable of driving IFN signaling ^{19,20} and as a co-activation of cGAS ^{21,22},
- 69 while also bearing the ability to counteract cGAS-STING activation ²³. This suggests that DNA-
- 70 PK regulates cGAS-STING pathway activation at several levels. Here, we tested whether DNA-
- 71 PK regulates inflammatory responses downstream of cGAS.
- To this aim, we used T98G glioblastoma cells that do not express detectable cGAS levels ²².
- 73 T98G cells were treated with the 2'3'-cGAMP CDN in the presence or absence of NU7441, a
- selective DNA-PK inhibitor ²⁴. Western blot (WB) analyses showed the expected STING-
- dependent signaling activation in the presence of 2'3'-cGAMP, as demonstrated by STING
- degradation, as well as phosphorylation of STING and IRF3 (Fig. 1a). Analyses of the
- expression of transcripts associated with STING activity, such as IFNB1, ISG15, IFIT1, and
- 78 CCL5 also showed the expected increase in response to 2'3'-cGAMP-mediated stimulation
- 79 (Fig. 1b). Interestingly, treatment with 2'3'-cGAMP in combination with NU7441 led to
- increased pSTING and pIRF3 levels (Fig. 1a) and enhanced the expression of IFNB1, ISG15,
- 81 *IFIT1*, and *CCL5*, as compared to treatment with 2'3'-cGAMP alone (Fig. 1b). To assess
- whether 2'3'-cGAMP in combination with NU7441 led to a biologically-relevant enhancement
- of type I IFN responses, we tested its impact on infection with the herpes simplex virus 1 (HSV-

1) DNA virus known to be sensitive to type I IFN responses ²⁵. We treated T98G cells with 2'3'-cGAMP and NU7441 individually or in combination prior to infection with a green fluorescence protein (GFP)-encoding HSV-1 molecular clone (HSV-1-GFP) and assessed the percentage of GFP-positive cells. We found that NU7441 boosted the inhibitory impact of 2'3'-cGAMP on HSV-1-GFP infection compared to treatment with 2'3'-cGAMP alone, attesting to an enhancement of the antiviral status of cells by the combination of 2'3'-cGAMP and NU7441 (Fig. 1c). These results indicate that inhibition of DNA-PK leads to enhanced 2'3'-cGAMP-associated signaling and antiviral activity, suggesting that DNA-PK may inhibit 2'3'-cGAMP

signaling in T98G cells.

DNA-PK is a holoenzyme comprised of three subunits. KU70 and KU80 form heterodimers that ensure the recruitment of the DNA-PK catalytic subunit (DNA-PKcs) to nuclear double-strand breaks to ensure repair by non-homologous end-joining ²⁶, but also to cytosolic dsDNA to participate to type I IFN signaling ²². Because NU7441 specifically inhibits the DNA-PKcs subunit of DNA-PK, our data suggest that DNA-PKcs may be sufficient to mediate the inhibition of 2'3'-cGAMP-associated signaling. We thus next used small interfering RNAs (siRNAs) targeting DNA-PKcs or the KU70 subunits of DNA-PK (Extended data Fig. 1a-b) and assessed the impact on 2'3'-cGAMP-dependent STING activation. Treatment with 2'3'-cGAMP following knock-down of DNA-PKcs, but not of KU70, led to increased expression of STING-associated transcripts such as *IFNB1*, *ISG15*, *IFIT2* and *CCL5* (Extended data Fig. 1c), phenocopying the effect of treatment with NU7441. Hence, our data supports that the absence of DNA-PKcs is sufficient to enhance 2'3'-cGAMP-associated type I IFN responses.

DNA-PKcs-dependent control of inflammatory responses operates upstream of STING

We next asked at which level the DNA-PKcs-mediated inhibition of 2'3'-cGAMP signaling operates. The fact that this phenotype can be observed in T98G cells that lack cGAS expression suggests that DNA-PKcs operates downstream of cGAS but upstream of STING.

To confirm this observation, we next used THP-1 myeloid cells that are cGAS and STING proficient, as well as THP-1 cells knock-out for cGAS (THP-1^{cGAS-/-}) or STING (THP-1^{STING-/-}). Control THP1 cells (THP-1^{CTRL}), THP-1^{cGAS-/-} and THP-1^{STING-/-} were mock treated or treated with 2'3'-cGAMP and NU7441 individually or in combination. Gene expression and WB analyses showed that combining 2'3'-cGAMP treatment with DNA-PK inhibition boosted the activation of STING-dependent signaling in THP-1^{CTRL} but also in THP-1^{cGAS-/-}, resulting in

increased expression of *IFNB1*, *ISG15*, *CXCL10*, and *IFIT2* (Fig. 1d) and increased phosphorylation of IRF3 and STING (Fig. 1e, lanes 1-4 and 5-8). In STING-deficient THP-1 cells, the 2'3'-cGAMP-associated response was abrogated, regardless of NU7441 treatment (Fig. 1d and e, lanes 9-12). Similar results were obtained in T98G cells engineered to be knocked-out for STING (T98G^{STING-/-}) where the absence of STING disrupted the impact of 2'3'-cGAMP treatment alone or in combination with DNA-PK inhibition, as attested by the absence of *IFNB1*, *ISG15*, *IFIT1*, *CCL5*, and *IFIT2* expression (Extended data Fig. 1d) and absence of phosphorylation of IRF3 and STING (Extended data Fig. 1e). These data support that DNA-PKcs-mediated inhibition of 2'3'-cGAMP signaling is independent of cGAS but requires the presence of STING.

We next assessed whether DNA-PKcs-associated regulation of cGAMP-dependent type I IFN responses may result from STING activation and subsequent type I IFN responses though stimulation of the Interferon-α/β receptor (IFNAR). To this aim, T98G cells were engineered to be knock-out for IRF3 (T98G^{IRF3-/-}) or IFNAR (T98G^{IFNAR-/-}). Those cell lines as well as control T98G cells (T98G^{CTRL}) were mock-treated or treated with 2'3'-cGAMP and NU7441, individually or in combination. As expected, IRF3 knock-out did not alter STING phosphorylation in response to 2'3'-cGAMP transfection (Extended data Fig. 1f). Importantly, we found that the potentiation of STING phosphorylation when 2'3'-cGAMP and NU7441 treatments were combined was not altered in absence of IRF3 (Extended data Fig. 1f). Similar experiments were conducted in T98G^{IFNAR-/-} cells, showing that absence of IFNAR did not prevent increased IRF3 and STING phosphorylation when T98G cells are treated with 2'3'-cGAMP in combination with NU7441 (Extended data Fig. 1g).

These data demonstrate that DNA-PKcs-dependent regulation of 2'3'-cGAMP-mediated inflammatory responses requires STING and is not a consequence of STING-dependent type I IFN responses and therefore operates upstream of STING activation.

DNA-PKcs interacts with 2'3'-cGAMP

Since DNA-PKcs exerts its inhibitory effect downstream of cGAS and upstream of STING, we hypothesized that DNA-PKcs may directly regulate 2'3'-cGAMP levels and therefore decrease STING activation. To test this hypothesis, we next used human embryonic kidney HEK293T cells to generate control (293T^{CTRL}) and DNA-PKcs knock-out (293T^{DNA-PKcs-/-}) cell lines. Indeed, HEK293T cells express low levels of cGAS and STING and therefore do not mount

measurable type I IFN responses when DNA repair is impeded by DNA-PKcs knock-out 146 (Extended data Fig. 2a). 293T^{CTRL} and 293T^{DNA-PKcs-/-} were treated with 2'3'-cGAMP prior to 147 assessment of intracellular 2'3'-cGAMP levels by enzyme-linked immunosorbent assay 148 (ELISA). We found that the absence of DNA-PK resulted in increased 2'3'-cGAMP levels (Fig. 149 2a). Similarly, in T98G cells were treated with 2'3'-cGAMP in the presence or absence of 150 NU7441, we found that in T98G cells, treatment with NU7441 increased intracellular 2'3'-151 cGAMP levels (Extended data Fig. 2b). These data suggest that increased STING activation 152 following DNA-PKcs inhibition may result from increased availability of 2'3'-cGAMP. 153 We next hypothesized that DNA-PKcs may regulate 2'3'-cGAMP levels through physical 154 interaction. We thus tested the capacity of 2'3'-cGAMP to interact with DNA-PKcs. To this 155 aim, we first immunoprecipitated DNA-PKcs from T98G cells using a DNA-PKcs-specific 156 antibody or control IgG (Extended data Fig. 2c). Immunoprecipitates were incubated with 2'3'-157 cGAMP prior to release using proteinase K and measurement of 2'3'-cGAMP. We found that 158 the DNA-PK immunoprecipitation presented a significant enrichment in bound 2'3'-cGAMP, 159 as compared to control (Fig. 2b). Similar results were obtained when FLAG-160 immunoprecipitating a FLAG-tagged DNA-PKcs over-expressed in HEK293T cells (Extended 161 data Fig. 2d-e). Of note, consistent with our observation that KU heterodimers are not necessary 162 for the DNA-PKcs-mediated inhibition of 2'3'-cGAMP signaling, no KU80 was detected in the 163 DNA-PKcs immunoprecipitation (Extended data Fig. 2e). To exclude further the participation 164 of DNA-PKcs co-factors in the binding to 2'3'-cGAMP, we next performed similar 165 166 experiments using recombinant DNA-PKcs, which was bead-immobilized using a DNA-PKcsspecific antibody (Extended data Fig. 2f) prior to incubation with 2'3'-cGAMP, release and 167 168 measurement of recovered 2'3'-cGAMP. We found a significant enrichment of 2'3'-cGAMP, when DNA-PKcs was present in the reaction (Fig. 2c), confirming that DNA-PKcs can interact 169 170 with 2'3'-cGAMP. Of note, when similar experiments were conducted using the 2'5'-GpAp 171 linear dinucleotide analog of 2'3'-cGAMP (thereafter, linear-cGAMP) that does not activate 172 STING (Invivogen), we did not retrieve detectable amounts of linear cGAMP in the DNA-PKcs immunoprecipitates (Extended Fig. 2g-h). 173 We next aimed to identify the domain of DNA-PKcs engaged in interaction with 2'3'-cGAMP. 174 Owing to the size of DNA-PKcs we first performed in silico molecular modelling and docking 175 analyses to identify putative binding regions. We used the resolved crystal of human DNA-176 PKcs (PDB: 5LUQ) as a starting biological system for docking analyses using 2'3'-cGAMP. 177 This predicted that 2'3'-cGAMP can dock into DNA-PKcs catalytic pocket (Fig. 2d and 178

180

181

182

183

184

185

186

187

188

189

190

191

192

193

194

195

196

197

198

199

200

201

202

203

204

205

206

207

209

Extended data Fig. 3a-b), adopting a stable conformation (Energy -28911.06 Kcal/mol, Table I) notably through strong H-bonds between residues Asp3723, Arg3741, His1069 and Asp3744, Arg3746, His3748 with the phosphodiester bonds within the 2'3'-cGAMP molecule (Extended data Fig. 3c). Congruent with our binding assays, in silico molecular modeling experiments performed with linear-cGAMP showed that the increased flexibility of linear-cGAMP as compared to 2'3'-cGAMP rendered this molecule unstable in the catalytic site of DNA-PKcs (Extended data Fig. 3d-e). The specificity of the performed in silico analyses was controlled using other DNA-repair-related enzymes belonging to the phosphatidylinositide 3-kinase (PI3K)-related kinase family, to which DNA-PK belongs, namely Ataxia Telangiectasia Mutated (ATM) and Ataxia Telangiectasia and Rad3-related protein (ATR), and thus possess analogous catalytic sites competent for ATP hydrolysis. The structures of ATM and ATR were modelled prior to the superposition of the catalytic sites with that of DNA-PKcs and comparative analysis of their catalytic cleft, predicting that 2'3'-cGAMP is unlikely to interact with these catalytic domains (Extended data Fig. 4a-b). Altogether, these in silico data confirm that 2'3'-cGAMP can bind selectively to DNA-PKcs and suggest that this interaction is likely to occur in the catalytic pocket of DNA-PKcs.

To verify the prediction that 2'3'-cGAMP interacts with DNA-PKcs catalytic pocket, two approaches were used. First, we assessed whether 2'3'-cGAMP alters DNA-PKcs catalytic activity *in vitro*. We found that 2'3'-cGAMP inhibits the ability of DNA-PKcs to hydrolyze ATP in a dose-dependent manner (Fig. 2e), suggesting that 2'3'-cGAMP can prevent the association of DNA-PKcs with its ATP substrate. To further confirm this association, we next used recombinant DNA-PKcs in immunoprecipitation assays, in which NU7441 was used as a competitor. We found that NU7441 was capable of displacing the interaction of 2'3'-cGAMP with DNA-PKcs (Fig. 2f), supporting that the interaction of 2'3'-cGAMP with DNA-PKcs occurs in its catalytic cleft.

Altogether, our data show that 2'3'-cGAMP interacts with the catalytic cleft of DNA-PKcs and suggest that this interaction may reduce the bioavailability of 2'3'-cGAMP for STING activation.

DNA-PKcs regulates the activity of 3'3'-cGAMP

To date, mammalian regulators of 2'3'-cGAMP have been shown to operate selectively ¹³⁻¹⁵.

We questioned the spectrum of DNA-PKcs activity on CDNs of bacterial origin. To account

for potential activation bias incurred by the treatment of cells with bacterial CDNs, we first 210 assessed the impact of three distinct bacterial CDNs on DNA-PKcs catalytic activity in vitro. 211 We used 3'3'-cGAMP ²⁷, bis-(3'-5')-cyclic dimeric adenosine monophosphate (c-di-AMP) and 212 bis-(3'-5')-cyclic dimeric guanosine monophosphate (c-di-GMP) ^{28,29}, all of which reportedly 213 are able to induce STING-dependent signaling. We found that, similar to what was observed 214 for 2'3'-cGAMP, 3'3'-cGAMP, but not c-di-AMP nor c-di-GMP, inhibited DNA-PKcs 215 catalytic activity in a dose-dependent manner (Fig. 3a and Extended data Fig. 5a). We next 216 assessed the binding of 3'3'-cGAMP and c-di-AMP to recombinant DNA-PKcs. We found that 217 DNA-PKcs was able to interact with 3'3'-cGAMP but not with c-di-AMP (Fig. 3b). In silico 218 docking analyses confirmed that 3'3'-cGAMP, but not c-di-AMP nor c-di-GMP, can interact 219 with DNA-PKcs in its catalytic cleft adopting a stable conformation (Energy -30182.10 220 Kcal/mol, Table I). Congruent with the apparent higher potency of 3'3'-cGAMP at inhibiting 221 DNA-PKcs, as compared to 2'3'-cGAMP (compare Fig. 2e and Fig. 3a), energies predicted for 222 the interaction in silico were slightly higher for the 3'3'-cGAMP:DNA-PKcs complex as 223 224 compared to the 2'3'-cGAMP:DNA-PKcs complex (Table I).

To further test the functional interaction between DNA-PKcs and 3'3'-cGAMP, we next treated T98G and THP-1 cells with 3'3'-cGAMP alone or in combination with NU7441. We found that combining 3'3'-cGAMP-treatment with DNA-PKcs inhibition enhanced STING phosphorylation (Fig. 3c and Extended data Fig. 5b) in both T98G and THP-1 cells and led to increased expression of STING activity-associated transcripts, namely *IFNB1*, *IFIT1*, *ISG15*, and *CCL5* in T98G (Fig. 3d) and THP-1 cells (Extended data Fig. 5c), as compared to cells treated only with 3'3'-cGAMP. Combined, our data show that DNA-PKcs selectively interacts with 3'3'-cGAMP and inhibits its capacity to activate STING-dependent signaling, but does not appear to interfere with other tested bacterial CDNs.

DNA-PKcs inhibits the activity of STING targeting drugs

225

226

227

228

229

230

231

232

233

234

STING is an important biomedical target for which a plethora of agonists are tested in ongoing clinical trials {Hines, 2023 #40}. Because several of these compounds have been designed based on the structure of CDNs capable of activating STING, we tested whether DNA-PKcs affects their potency. To this aim, T98G cells were treated with STING agonists individually or in combination with NU7441. The tested STING agonists were: ADU-S100,diABZI, and E7766.

We first investigated the impact of DNA-PK on diABZI and E7766 which are STING agonists 241 designed based on the structure of 2'3'-cGAMP. WB analyses showed that treatment with 242 E7766 or diABZI in combination with NU7441 led to enhanced IRF3 and STING 243 phosphorylation (Fig. 4a and extended data Fig. 6a) and increased expression of IFNB1, ISG15, 244 IFIT1 and CCL5, compared to STING agonists alone (Fig. 4b and extended data Fig. 6b). In 245 order to assess whether the increased potency of E7766 upon DNA-PKcs inhibition results from 246 its interaction with DNA-PKcs, we measured DNA-PKcs-mediated ATP hydrolysis activity in 247 the presence of increasing doses of E7766 in vitro. We found that E7766 potently inhibited 248 249 DNA-PKcs activity (Fig. 4c), supporting a similar mechanism of action than that measured for 2'3'-cGAMP and 3'3'-cGAMP (Fig. 2-3). 250 Next, we assessed the impact of DNA-PKcs on ADU-S100, a compound that was designed 251 based on ci-d-AMP. In contrast to data obtained with E7766 or diABZI, treatment with ADU-252 S100 in combination with NU7441 lead to non-significant enhancement of ADU-S100-induced 253 STING activation as shown by WB (Fig. 4d) or gene expression analysis (Fig. 4e). Furthermore, 254 in vitro DNA-PKcs ATP hydrolysis assays also showed that ADU-S100 fails to inhibit DNA-255 PKcs catalytic activity (Fig. 4f). These data thus show that DNA-PKcs inhibition selectively 256 alters the efficiency of STING agonists. 257 258 Finally, we sought to assess whether DNA-PKcs-mediated inhibition of these compounds could influence the establishment of physiologically relevant STING-associated biological responses, 259 260 namely antiviral responses. To this aim, we treated T98G cells with STING agonists individually or in combination with NU7441, followed by infection with either HSV-1-GFP or 261 262 a GFP reporter expressing vesicular stomatitis virus (VSV-GFP). The latter is a RNA virus known to be sensitive to type I IFN responses ³⁰. In agreement with previous reports ²⁵, 263 treatment with STING agonists decreased infection by both VSV-GFP and HSV-1-GFP (Fig. 264 4g-h and Extended data Fig. 6c-d). Combining such treatments with NU7441-mediated DNA-265 PKcs inhibition led to a more profound decrease of the percentage of VSV-GFP and HSV-1-266 GFP infected cells (Fig. 4g-h and Extended data Fig. 6c-d). Our data therefore support that 267 DNA-PKcs can inhibit the capacity of STING agonists to induce a STING-dependent antiviral 268 269 responses.

Discussion

272

273

274

275

276

277

278

279

280

281

282

283

284

285

286

287

288

289

290

291

292

293

294

295

296

297

298

299

300

301

302

In this study, we show that DNA-PKcs controls 2'3'-cGAMP and 3'3'-cGAMP CDNsassociated inflammatory response. Our data supports a model in which DNA-PKcs operates by binding to those CDNs selectively, decreasing their availability for interaction with STING and thereby buffering their STING-associated activity. This finding is in contrast with other mechanisms described to control CDN activity that appear to have specifically evolved to control extracellular 2'3'-cGAMP levels ¹³⁻¹⁵, which is the only CDN described to date to be produced by mammalian cells ⁷. The fact that DNA-PKcs can counteract the impact of 3'3'cGAMP on immunity seems to be a distinctive feature and may have evolved as a mechanism of tolerance towards 3'3'-cGAMP-producing bacteria. Phylogenetic analyses have shown that DNA-PKcs is highly conserved ³¹, suggesting that this mechanism of action may be present across the tree of life and may operate as a general mechanism to prevent overactivation of inflammatory responses. We and others have reported that DNA-PK can operate as a co-activator of cGAS-STING in the presence of cytosolic dsDNA ^{19,21,22} while others reported an inhibitory role of DNA-PK on antiviral responses ²³. The present study supports that DNA-PK has a dual role in modulating cGAS-STING signaling, which could alter the amplitude and kinetics of dsDNA responses, as well as homeostatic inflammation. Importantly, we also demonstrate that 2'3'-cGAMP and 3'3'-cGAMP can block DNA-PKcs catalytic activity, which may have an impact on its ability to repair double-strand breaks. However, previous studies have shown that of the levels of DNA-PK do not correlate with DNA repair functions ³² and that other pathways can take over NHEJ-mediated repair when DNA-PKcs is non-functional ³³. While the impact of CDNs on DNA-PK-specific repair functions, such as its role in micronuclei damage ³⁴, remain to be dissected, our findings also support that, as previously speculated ^{35,36}, the role of DNA-PKcs may not be confined to DNA repair. Indeed, several reports point towards multifunctional roles of DNA-PK, highlighting in particular its multi-level involvement in the regulation of inflammatory responses ³⁶. Importantly, our study also shows that the ability of DNA-PKcs to control CDN-associated inflammatory responses is very relevant for drugs designed on CDN-based scaffolds. Because such compounds are being clinically tested, it is essential to investigate their off-target effects that may lead to confounding results. For instance, it is important to assess whether these compounds may bear an increased ability to interact with DNA-PKcs, thereby inducing DNA repair deficiency-associated side-effects. Conversely, the status of DNA-PK in target tissues

may be important to assess in order to predict the capacity of STING agonists to induce beneficial inflammation. This is particularly relevant in the context of cancer immunotherapy where STING agonists are used to boost inflammatory responses ³⁷. Cancer types presenting DNA-PKcs anomalies, such as copy number variations are frequent ³⁸. In those contexts, our data strongly suggests that the impact of STING agonists may be altered. It is therefore important to take into account the status of DNA-PKcs in cancer patients enrolled in STING-agonist-based clinical trials for better stratification.

References

Tables

Table I. ALL: complex energy; INT: interaction energy; VDW: Van der Waals. Calculated energies are expressed in kcal.mol-1

		Energy	Strain	VDW	Electrostatic
2'3'-cGAMP	ALL	-28911.06	1388.79	6972.41	-38159.41
	INT	-172.03	0.00	34.28	-206.31
3'3'-cGAMP	ALL	-30182.10	1050.79	6169.34	-38204.66
	INT	-252.10	0.00	-40.74	-21.35

Figures and Legends

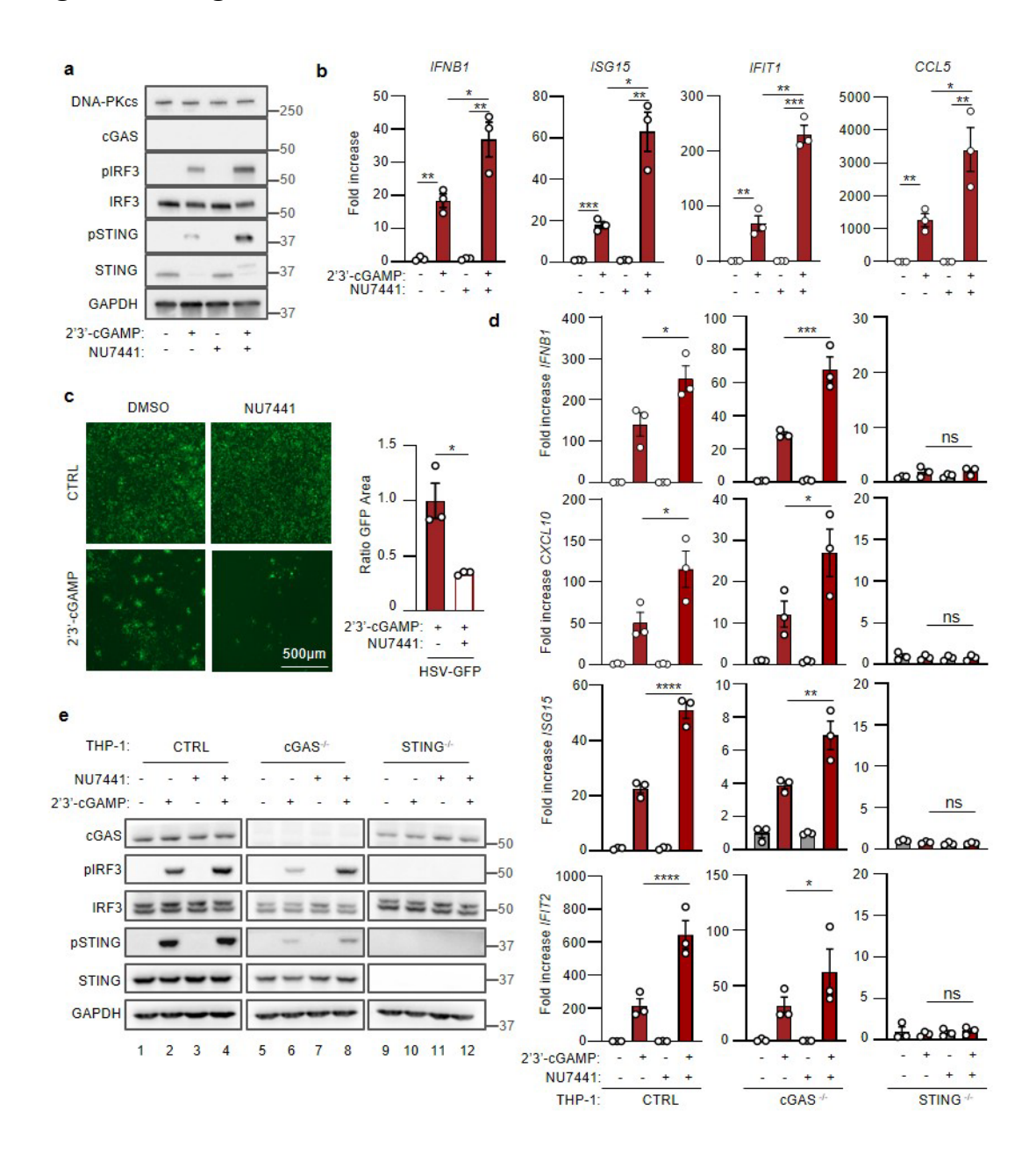


Figure 1. DNA-PK inhibits 2'3'-cGAMP signaling. a, T98G cells were treated or not with $2\mu M$ the NU7441 DNA-PKcs inhibitor for 1 hour prior to transfection or not of $10\mu g/ml$ 2'3'-cGAMP for 6 hours and analysis of whole cell extract by Western blot (WB) using the indicated antibodies. WB is representative of at least 3 independent experiments. **b,** As in **a,** except that gene expression analysis was conducted. Graphs present the mean \pm standard error from the mean (SEM) of 3 independent experiments. **c,** T98G cells were pretreated or not for 1 hour with $2\mu M$ NU7441 prior to transfection of $10\mu g/ml$ 2'3'-cGAMP for 6 hours prior to infection with HSV-1-GFP. Images are representative of 3 independent experiments. Graphs shows the relative change of the GFP signal between the indicated conditions, following normalization to

their own controls in 3 independent experiments. **d**, THP-1 cells expressing a control gRNA (CTRL), or cGAS- or STING-targeting gRNAs were treated or not with 2µM of the NU7441 DNA-PKcs inhibitor for 1 hour prior to transfection of not of 10µg/ml 2'3'-cGAMP for 6 hours and gene expression analysis. Graphs present the mean (±SEM) of 3 independent experiments. **e**, As in **d** except that whole cell extracts were analyzed by WB using the indicated antibodies. WB are representative of 3 independent experiments. Statistical significance was calculated by Student T-test. ****: p<0.0001; ***: p<0.001; **: p<0.05; ns: not significant.

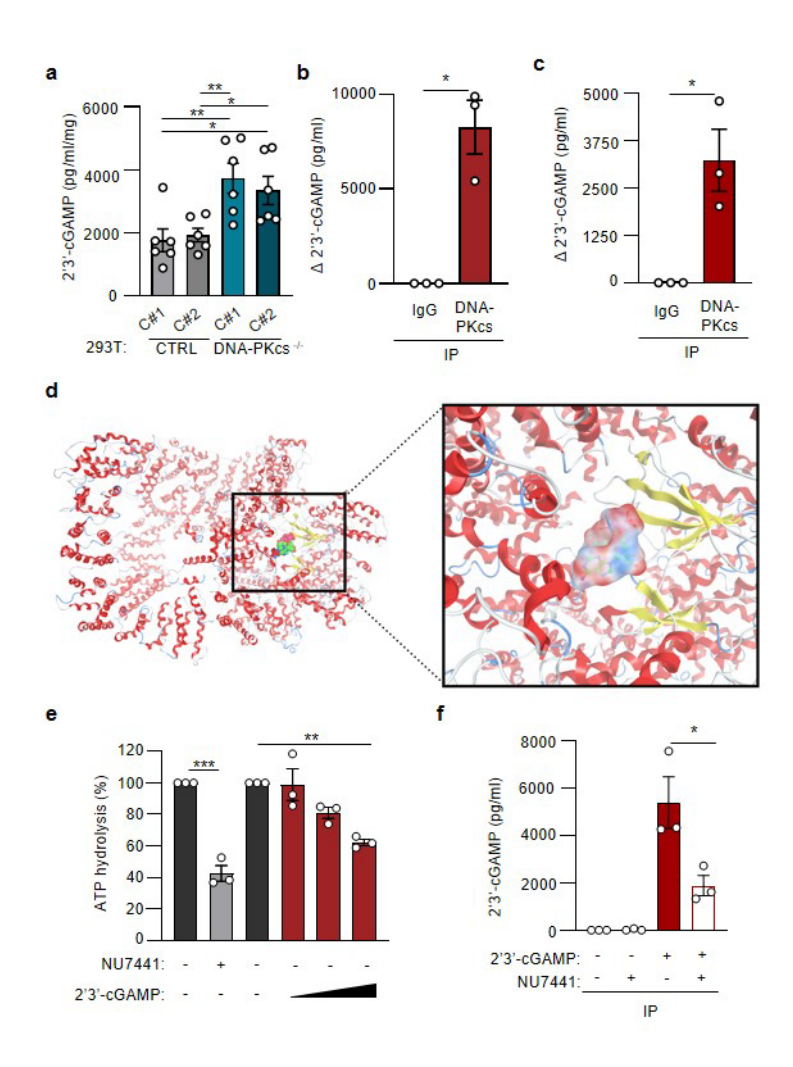


Figure 2. 2'3'-cGAMP interacts with DNA-PKcs catalytic pocket. a. 293T cells expressing control gRNA or DNA-PKcs-targeting gRNAs were transfected with 10μg/ml 2'3'-cGAMP for 3 hours prior to measurement of intracellular 2'3'-cGAMP levels. The graph presents the increased 2'3'-cGAMP levels as measured from 6 independent experiments. b, Whole cell extracts from T98G cells were used to perform immunoprecipitations using either mock IgG to a DNA-PKcs-specific antibody prior to incubation of immunoprecipitates with 2'3'-cGAMP and measurement of bound 2'3'-cGAMP. Graph represents mean (±SEM) 2'3'-cGAMP levels

as measure in Mock and DNA-PK-specific IP. Graph presents the mean of 3 independent experiments. **c**, As in b, except that immunoprecipitation was performed on recombinant DNA-PK. Graph presents the mean (±SEM) of 3 independent experiments. **d**, Representation of the molecular modeling of 2'3'-cGAMP in interaction with DNA-PKcs. **e**, ATP hydrolysis by DNA-PK was measured in vitro in presence of NU7441 or increasing doses 300μM- 2700μM of 2'3'-cGAMP. Graph presents the mean of 3 independent experiments. **f**, As in d, except that the NU7741 inhibitor was used as a competitor. Statistical significance in a, c, d and f was calculated by Student T-test. A one-way Anova was performed for the 2'3'-cGAMP ramp in panel e. ***: p<0.001; **: p<0.01; *: p<0.05.

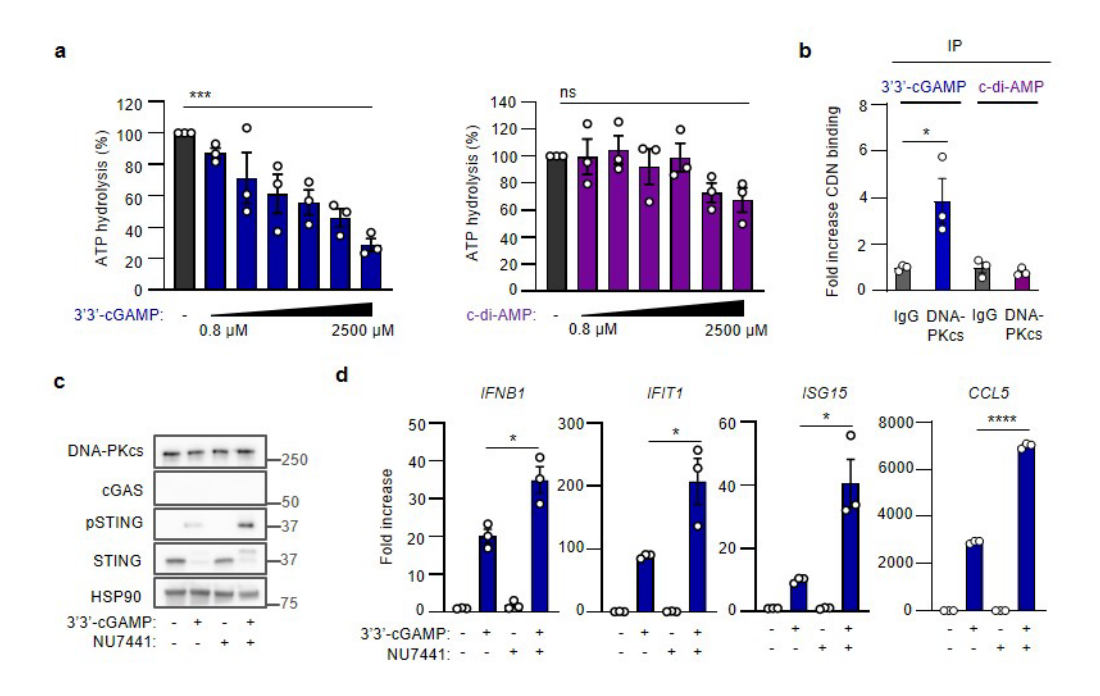


Figure 3. DNA-PKcs inhibits 3'3'-cGAMP-associated STING activation. a, ATP hydrolysis by DNA-PK was measured in vitro in presence of increasing doses (0.8 μM to 2500 μM) of 3'3'-cGAMP or c-di-AMP. Graph presents the mean of 3 independent experiments. Statistical significance was calculated by ANOVA. ***: p<0.001; ns: not significant. b, Recombinant DNA-PKcs was immunoprecipitated using either mock IgG to a DNA-PKcs-specific antibody prior to incubation with 3'3'-cGAMP or c-di-AMP and ELISA-based measurement of bound CDNs. Graph represents mean (±SEM) 2'3'-cGAMP levels as measure in Mock and DNA-PKcs-specific IP in 3 independent experiments. c. T98G cells were treated or not with 2μM NU7441 prior to addition or not of 10μg/ml fluorinated 3'3'-cGAMP for 6 hours and analysis of whole cell extracts by WB using indicated antibodies. WB are representative of at least 3 independent experiments. d, Gene expression analyses were conducted on T98G cells treated

as in **c**. Graphs present the mean (\pm SEM) of biological triplicates, representative of 3 independent experiments. Statistical significance was calculated by Student T-test. ****: p<0.0001; *: p<0.05.

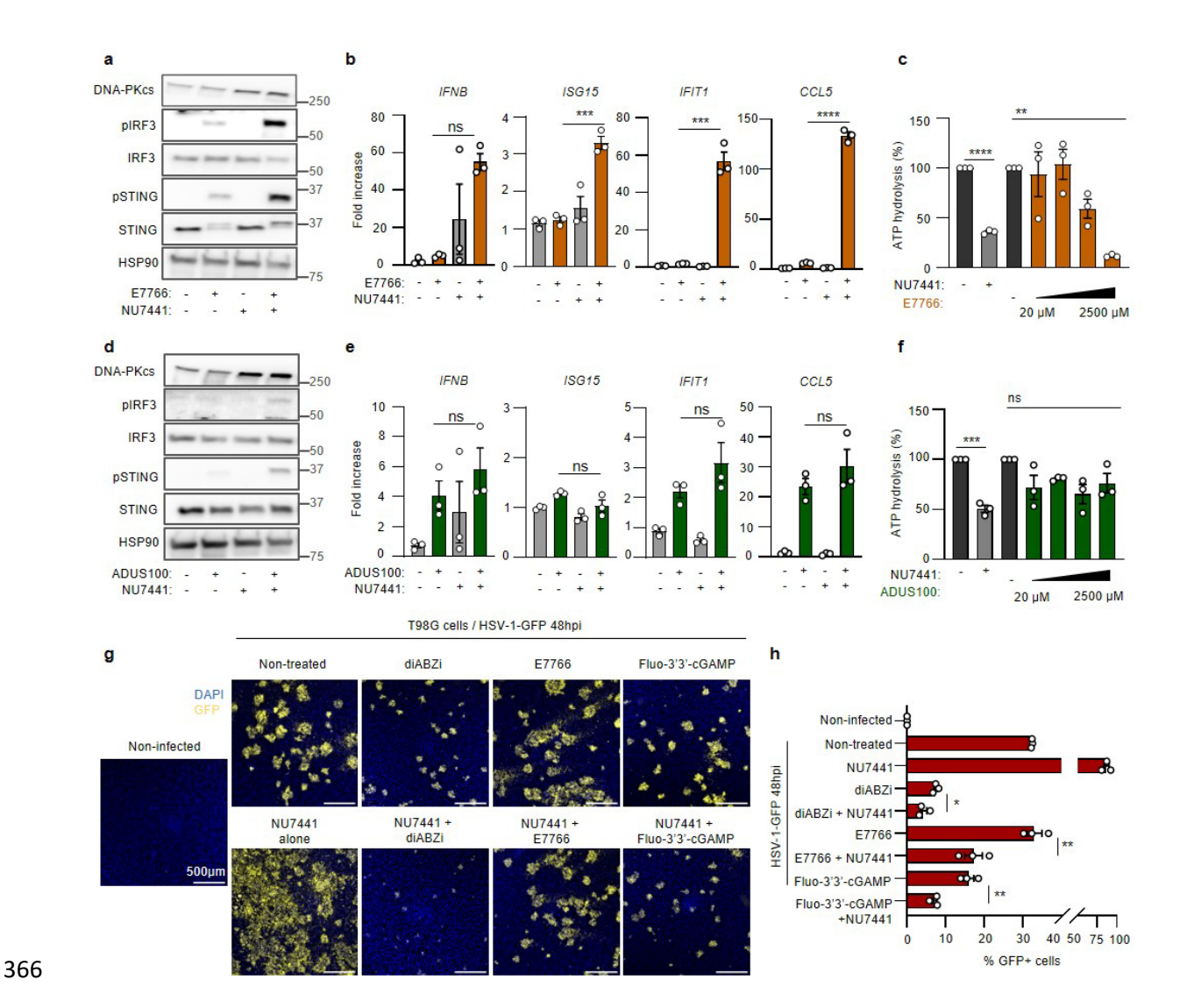


Figure 4. DNA-PKcs inhibits the activity of STING agonists. a, T98G cells were treated or not with $2\mu M$ of NU7441 prior to addition or not of $1\mu M$ of E7766 STING agonist for 3 hours and analysis of whole cell extracts by WB using indicated antibodies. WB is representative of at least 3 independent experiments. **b**, gene expression analyses were conducted on T98G cells treated as in **a**. Graphs present the mean (\pm SEM) of at least 3 independent experiments performed in biological triplicates. **c**, ATP hydrolysis by DNA-PK was measured *in vitro* in presence of increasing doses (0.8 μM to 2500 μM) of E7766. Graph presents the mean of 3 independent experiments. Statistical significance was calculated by one-way ANOVA for the E7766 ramp. **d**. T98G cells were treated or not with $2\mu M$ of NU7441 prior to addition or not of $50\mu M$ of the ADUS100 STING agonist for 3 hours and analysis of whole cell extracts by WB

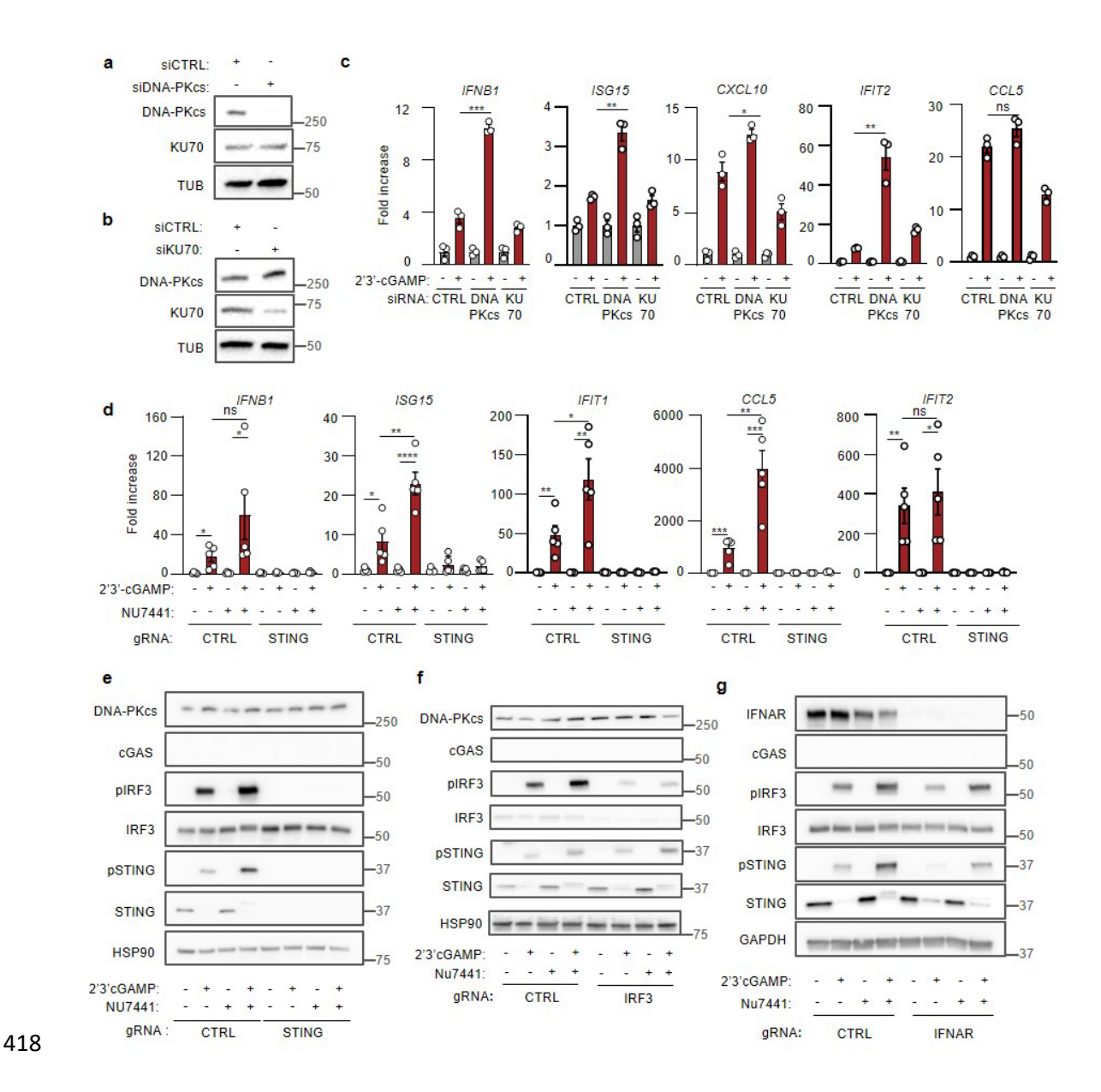
using indicated antibodies. WB is representative of at least 3 independent experiments. e, gene

377

expression analyses were conducted on T98G cells treated as in d. Graphs present the mean 378 (±SEM) of at least 3 independent experiments performed in biological triplicates. Statistical 379 significance was calculated by Student T-test. ns: not significant. f, ATP hydrolysis by DNA-380 PK was measured *in vitro* in presence of increasing doses (0.8 µM to 2500 µM) of ADU-S100. 381 Graph presents the mean of 3 independent experiments. Statistical significance was calculated 382 by one-way ANOVA for the ADU-S100 ramp. g, T98G cells were treated with the diABZI, 383 E7766 or fluorinated 3'3'-cGAMP agonists in combination of not with 2μM of NU7741. Cells 384 were subsequently infected or not with HSV-1-GFP for 48 hours, DAPI nuclear staining and 385 image acquisition. Images are representative of 3 independent experiments performed in 386 biological triplicates. h. Graph presents the quantification of GFP signal in experiments 387 conducted as in g. Statistical significance was calculated by Student T-test. Unless otherwise 388 stated. ****: p<0.0001; ***: p<0.001; *: p<0.01; *: p<0.05; ns: not significant. 389 **Acknowledgments:** We thank all members of the Molecular Basis of Inflammation laboratory 390 for their critical reading of this manuscript. We thank Caroline Bertin, Johanna Marines, Amel 391 Bouzid, Mathilde Saccas for technical assistance. We thank Soren Paludan for control, STING-392 and cGAS-deficient THP-1 cell lines and HSV-1-GFP. We acknowledge the MRI imaging 393 facility, member of the national infrastructure France-BioImaging infrastructure supported by 394 the French National Research Agency (ANR-10-INBS-04, "Investments for the future"). 395 396 This work was co-funded by the European Union (ERC, SENTINEL 101087092 to NL; DELV 101039538 to KM). Views and opinions expressed are however those of the author(s) only and 397 398 do not necessarily reflect those of the European Union or the European Research Council. 399 Neither the European Union nor the granting authority can be held responsible for them. This 400 work was also co-funded by : the ANR [AlphA(NL), dezincRNA to (KM)]; l'Institut National du Cancer INCa 1884 (NB)]; LA Ligue pour la recherche contre le cancer [AAPARN 401 2021.LCC/JuF (NL), équipe labellisée (NB)], the Agence Nationale de Recherche sur le SIDA 402 et les Hépatites virales (ANRS) [ECTZ117448 (NL) and fellowships to CT and JMK], the I-403 SITE Excellence Program of the University of Montpellier, under the Investissements France 404 2030 [RETTiNA (NL), ChoiCe (NL)], the Fondation ARC [ARCPJA2021060003720 405 COPALYS (NL), ARCPJA2021060003886 (NB)], La Région Languedoc Roussillon 406 [Prématuration 2021 MODULON 21015964 (NL)], Fondation de France [fellowship (JJ)] and 407 the Centre National de La Recherche Scientifique [Prématuration CNRS (NL)]. 408

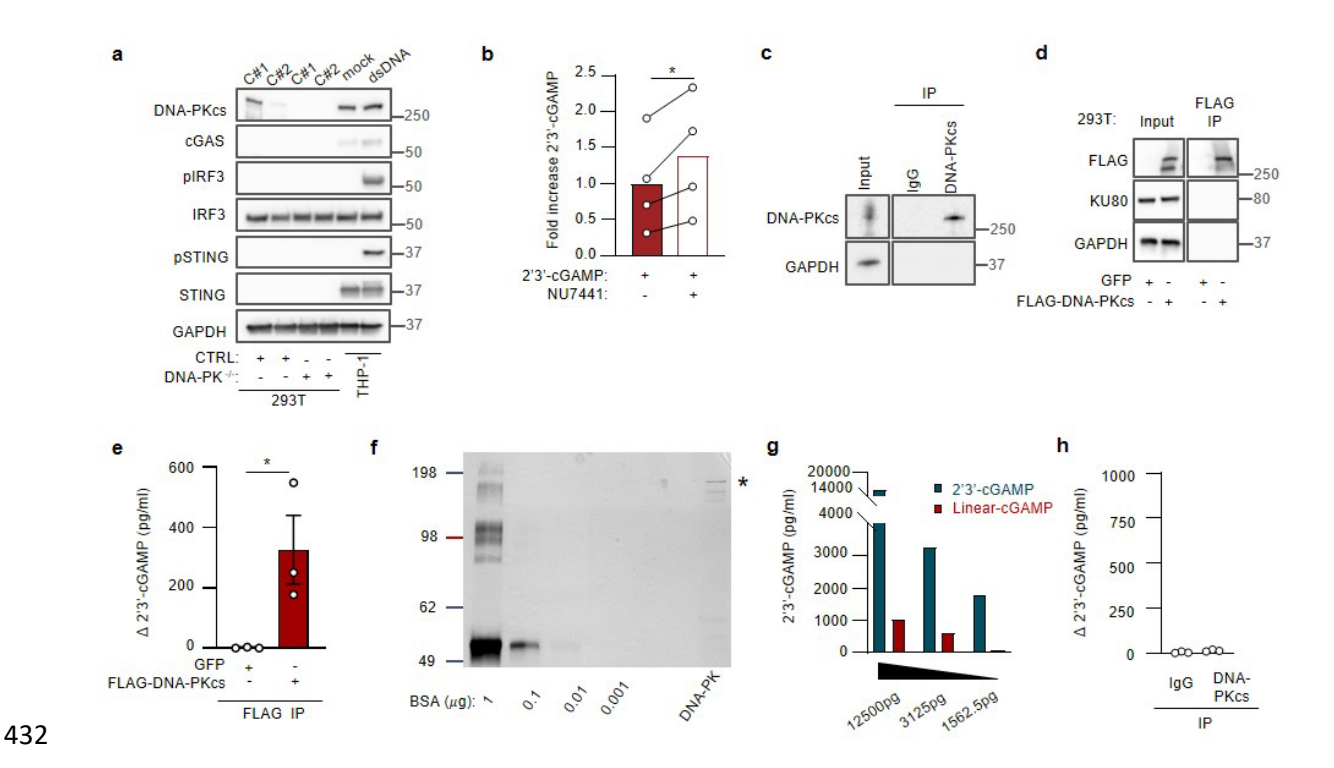
- **Author contributions:** Conceptualization: NL, DV; Methodology: CT, NL, DV; Investigation:
- 410 CT, IKV, MS, JJ; JMK, MC, IEM; Visualization: CT, DV, IKV, NL; Funding acquisition: NL,
- 411 KM, NB; Project administration: NL; Supervision: NL, DV, IKV, GPC, NB, KM; Writing –
- original draft: NL; Writing review & editing: NL, DV, CT, IKV, MS, JJ, JMK; KM, NB, DV.
- 413 **Competing interests:** Authors declare that they have no competing interests.
- 414 Materials and correspondence: Correspondence and requests for material should be
- addressed to Nadine Laguette and Dimitrios Vlachakis.

Extended data Figures and Legends



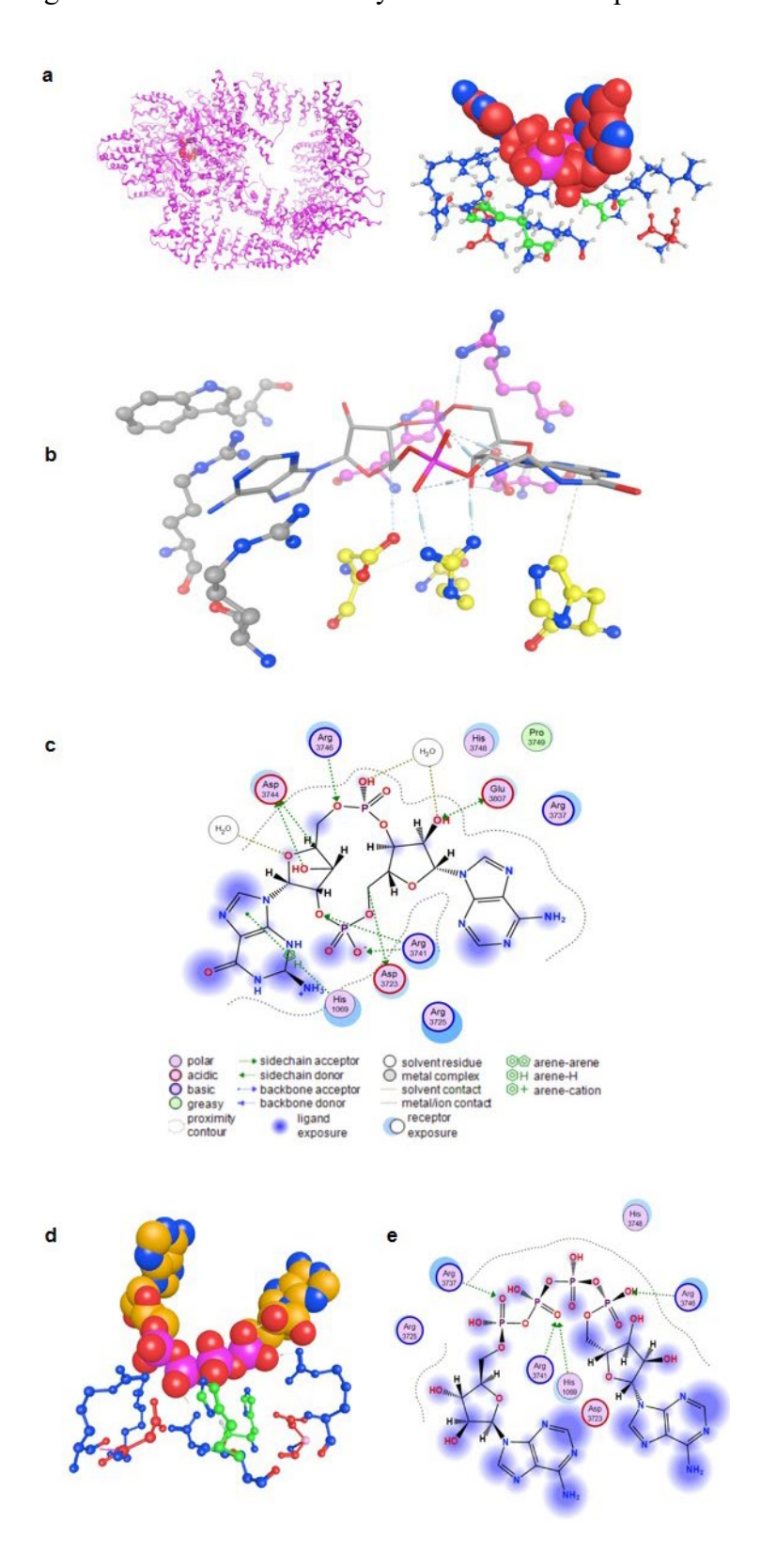
Extended data Figure 1. DNA-PK inhibits 2'3'-cGAMP signaling. a-b, T98G cells were transfected for DNA-PKcs- or KU70-targeting siRNA or a control non targeting siRNA for 48 hours prior analysis of knockdown efficiency by WB using the indicated antibodies. c, T98G cells were transfected for DNA-PKcs- or KU70-targeting siRNA or a control non targeting siRNA prior to transfection or not of 2'3'-cGAMP for 6 hours and gene expression analyses Graphs present the mean (±SEM) of 3 independent experiments. d, T98G cells engineered to express control non-targeting or STING-targeting gRNAs were treated or not with 2μM of NU7441 prior to Mock transfection or transfection of 10μg/ml 2'3'-cGAMP and gene expression analysis. e, as in d except that WB analysis was performed using the indicated antibodies. f, as in e, except that T98G cells expressing a IRF3-targeting gRNA were used. g,

as in **e**, except that T98G cells expressing an IFNAR-targeting gRNA were used. WB are representative of at least 3 independent experiments. Statistical significance was calculated by Student T-test. ***: p<0.001; **: p<0.01; *: p<0.05; ns: not significant.



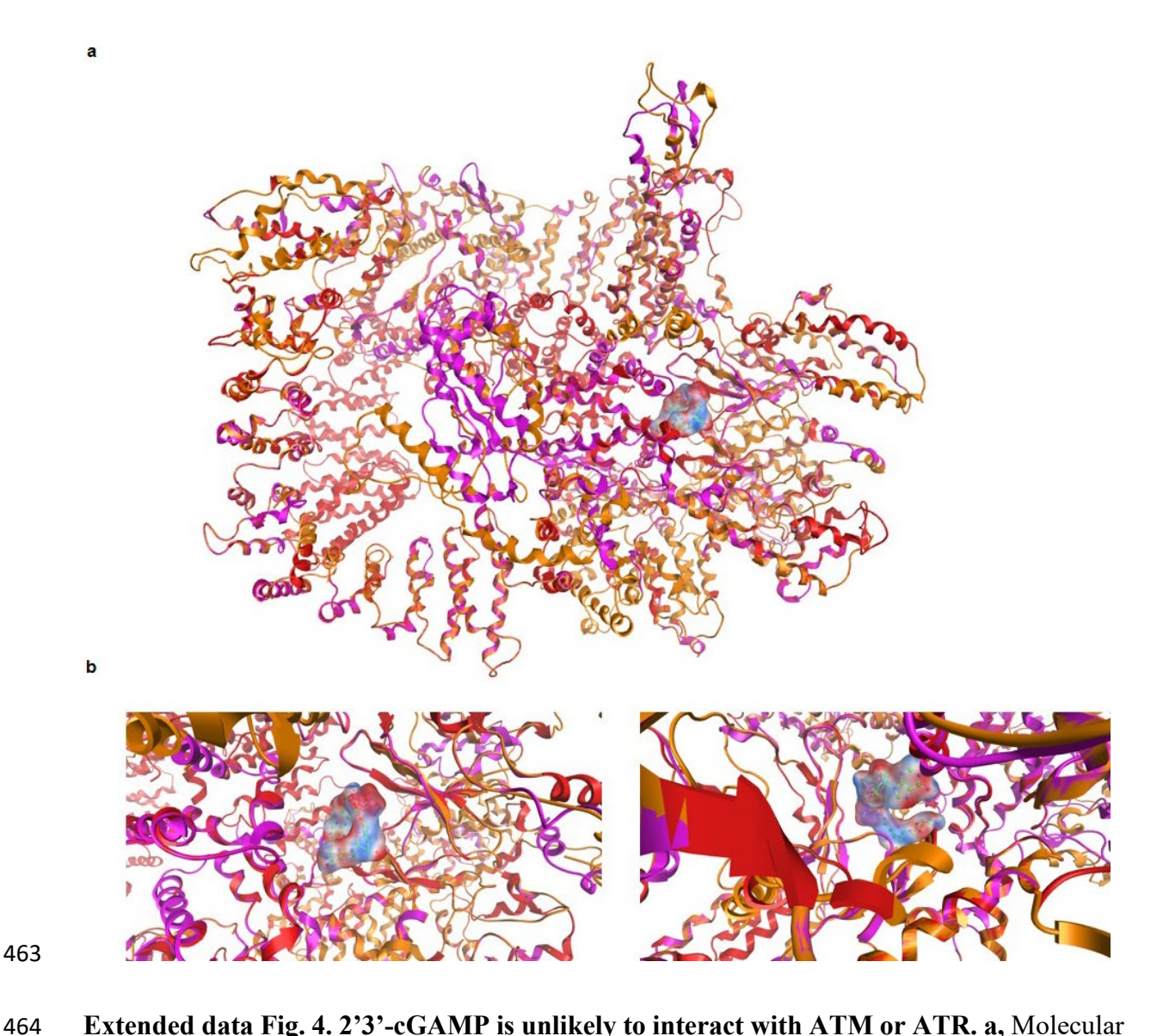
Extended data Fig 2. 2'3'-cGAMP interacts with DNA-PKcs. a, Whole cell extract of 293T cells engineered to express a control of DNA-PKcs-targeting gRNA were analyzed by WB using the indicated antibodies. C#: clone. b, T98G cells were treated with 2μM NU7741 for 1 hour prior to 2'3'-cGAMP transfection for 3 hours and analysis of intracellular 2'3'-cGAMP levels. Graph presents the mean (±SEM) of 4 independent experiments. c, WB analysis of DNA-PKcs IP used in Figure 2c was conducted using the indicated antibodies. d, FLAG-tagged DNA-PKcs was expressed in 293T^{DNA-PKcs-/-} (C#2) prior to FLAG immunoprecipitation. WB analysis of Input material and FLAG IP was conducted using the indicated antibodies. e. Immunoprecipitated material obtained as in d was incubated with 2'3'-cGAMP. Bound 2'3'-cGAMP was measured by ELISA. f, Silver-staining was conducted on immunoprecipitated recombinant DNA-PKcs used in figure 2. g, The detection range of linear-cGAMP as compared to 2'3'-cGAMP was estimated using ELISA. h, Recombinant DNA-PKcs was used to perform immunoprecipitations using either mock IgG to a DNA-PKcs-specific antibody prior to incubation of immunoprecipitates with Linear-cGAMP and measurement of bound 2'3'-cGAMP. Graph represents mean (±SEM) 2'3'-cGAMP levels as measure in Mock and DNA-

PKcs-specific IP. All WBs are representative of 3 independent experiments. Statistical significance was calculated by Student T-test. *: p<0.05.



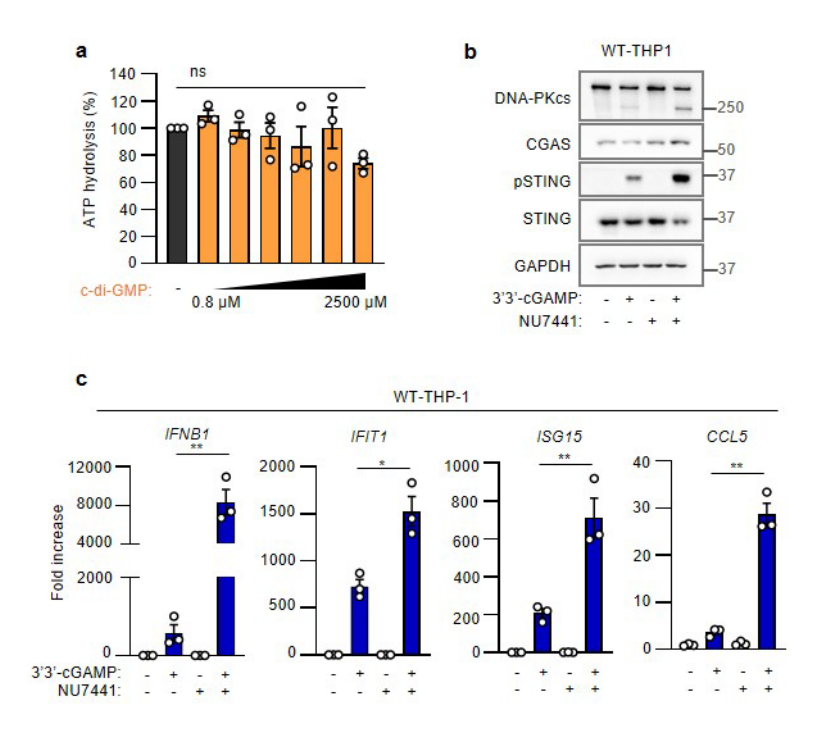
Extended data Fig. 3. 2'3'-cGAMP but not Linear-cGAMP is predicted to interact with the catalytic cleft of DNA-PKcs. a, Molecular modelling and docking study of 2'3'-cGAMP

into DNA-PKcs. Left: Human DNA-PKcs in ribbon representation with 2'3'-cGAMP docked in its catalytic site. Right: The docking conformation of 2'3'-cGAMP (in red spacefill representation) into the catalytic site of DNA-PKcs in the proximity of the catalytic residues (in ball and stick representation). **b**, The docked conformation adopted by 2'3'-cGAMP onto the catalytic site of DNA-PKcs upon the Molecular Dynamics simulations. **c**, The 2D molecular interactions diagram of 2'3'cGAMP with the catalytic residues of DNA-PKcs. **d**, Molecular modelling and docking study of the Linear-cGAMP into DNA-PKcs. The docking conformation of linear cGAMP (in spacefill representation) into the catalytic site of DNA-PKcs in the proximity of the catalytic residues (in ball and stick representation). **e**, The 2D molecular interactions diagram of Linear-cGAMP with the catalytic residues of DNA-PKcs.

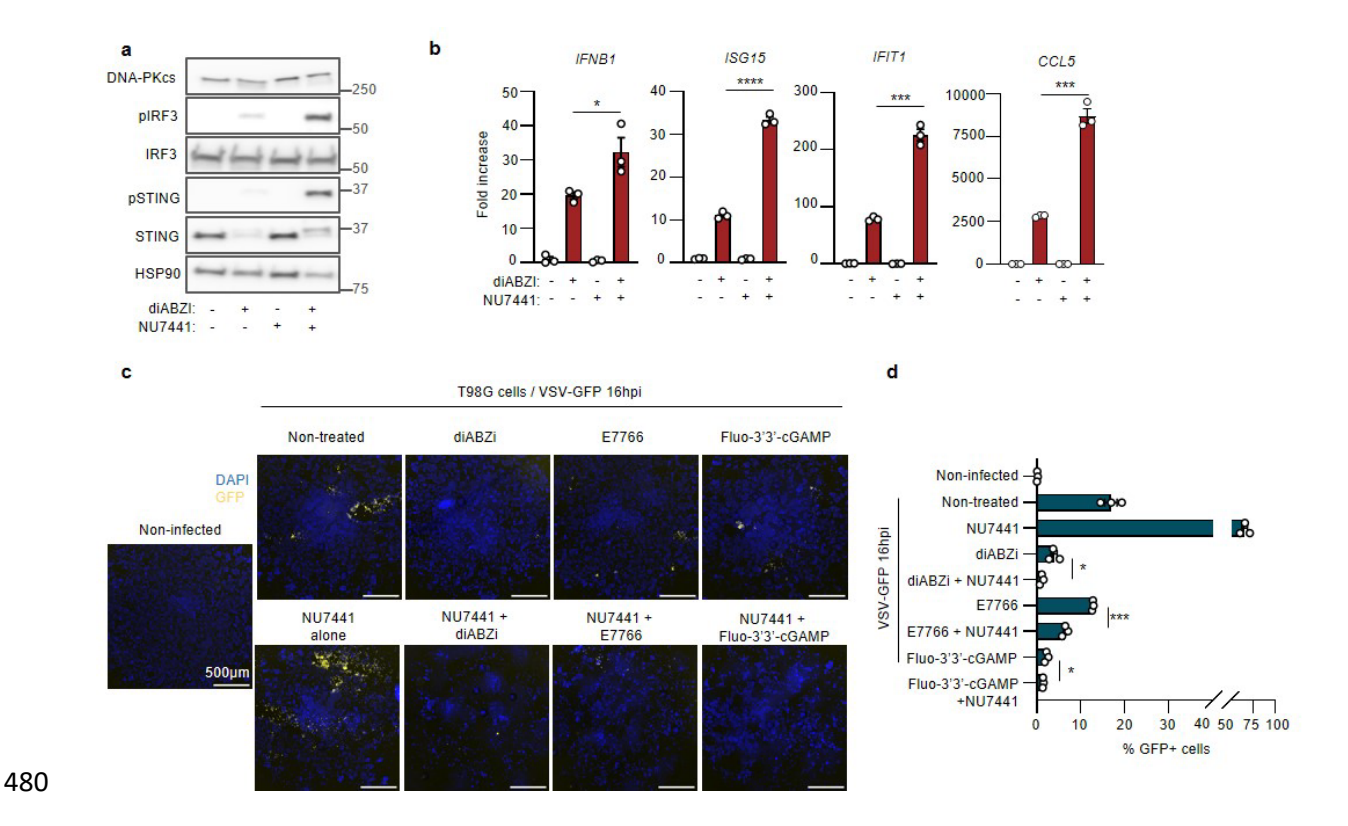


Extended data Fig. 4. 2'3'-cGAMP is unlikely to interact with ATM or ATR. a, Molecular modelling of ATM and ATR. DNA-PKcs superposed to the models of ATM and ATR (in red, magenta and orange ribbon representations respectively). b, Close-up of the superposed active

sites. Each of the 3 kinases has significant conformational differences and docking of 2'3'-cGAMP to all of them failed to return a thermodynamically viable pose (complex conformation).



Extended data Fig. 5. DNA-PKcs selectively counteracts CDNs. a, ATP hydrolysis by DNA-PKcs was measured in vitro in presence of increasing doses (0.8 μM to 2500 μM) of c-di-GMP. Graph presents the mean (±SEM) of 3 independent experiments. Statistical significance was calculated by one-way ANOVA. ns: not significant. b, THP-1 cells were treated or not with 2 μM NU7741 in combination or not with 10μg/ml fluorinated 3'3'-cGAMP for 6 hours prior to WB analysis using the indicated antibodies. WB is representative of 3 independent experiments. c, As in b, except that gene expression analyses were conducted. Graphs present the mean (±SEM) of 3 independent experiments performed in biological triplicates. Statistical significance was calculated by Student T-test. ***: p<0.001; **: p<0.01; *: p<0.05.



Extended Data Fig. 6. DNA-PKcs inhibits the activity of STING agonists. a, T98G cells were treated or not with 2μM NU7741 for 1 hour prior to addition or not of 10μM of diABZI for 3 hours prior to WB analysis using the indicated antibodies. WB are representative of at least 3 independent experiments. b, As in a, except that gene expression analyses were conducted. Graphs in c and e present the mean (±SEM) of 3 independent experiments performed in biological triplicates. Statistical significance was calculated by Student T-test. ****: p<0.0001; ***: p<0.001; **: p<0.05. c, T98G cells were treated with the diABZI, E7766 or 3'3'-cGAMP agonists in combination or not with 2μM of NU7441. Cells were subsequently infected or not with VSV-GFP for 16 hours, DAPI nuclear staining and image acquisition. Images are representative of 3 independent experiments performed in biological triplicates. d, Graphs present the quantification of GFP signal in experiments conducted as in c.

Methods

Cells and Cell Culture:

T98G cells were a gift from Caroline Goujon (IRIM, Montpellier, France). Control THP-1, cGAS-deficient THP-1 (THP-1^{cGas-/-}) and STING-deficient THP-1 (THP-1^{Sting-/-}) were a gift of S. R. Paludan (Aarhus university, Aarhus, Danemark). Vero (African green monkey),

- 498 HEK293T (*Homo sapiens*) and THP-1 (*Homo sapiens*) cells were obtained from the American
- 499 Type Culture Collection (ATCC).
- 500 T98G^{STING-/-}, T98G^{IRF3-/-} and their control counterparts were previously generated using the
- 501 CRISPR-Cas9 technology ²². Parental and genetically engineered T98G, HEK293T, and Vero
- cells were maintained in Dulbecco's Modified Eagle Medium (DMEM) supplemented with 10
- 503 % Fetal Bovine Serum (FBS, Eurobio), 1% L-glutamine (Lonza), 1% Penicillin/Streptomycin
- 504 (Lonza). THP-1 cells (Cat#TIB-202, ATCC) were cultured in Roswell Park Memorial Institute
- 505 (RPMI, Lonza) supplemented with 20% FBS, 1% penicillin/streptomycin and 1% L-glutamine.
- All cell lines were maintained at 37 °C, under 5% CO₂.
- 507 <u>Drugs:</u>
- 508 NU7441 Biotechne/Tocris, #3712, **CID:** 11327430
- 509 DMSO Sigma, D2650, CID: 679
- 510 2'3'-cGAMP InvivoGen, tlrl-nacga23-02, CID: 137120248
- 3'3'-cGAMP InvivoGen, tlrl-nacga, CAS number: 849214-04-6
- 512 c-di-AMP InvivoGen, tlrl-nacda, **CAS number:** 2734909-87-4 / 54447-84-6 (free acid)
- 513 c-di-GMP InvivoGen, tlrl-nacdg, CAS number: 2222132-40-1 / 61093-23-0 (free acid).
- 514 diABZI InvivoGen, tlrl-diabzi-2, CID: 137701219, CAS number: 2138299-34-8
- 515 E7766 MedChemExpress, HY-111999A,
- 516 ADUS100 ammonium salt MedChemExpress, HY-12885B
- 517 Fluorinated 3'3'-cGAMP Invivogen, tlrl-nacgaf-05, CAS number: not available
- Viral particle production and generation of knock-out cell lines
- To generate the T98G^{IFNAR-/-} knock-out and control cell lines, lentiviral particles were produced
- by co-transfection of 2×10^6 293T cells with 5 µg of LentiCRISPRv2GFP plasmid (Addgene #
- 82416) expressing the gRNA targeting the gene of interest or non-targeting control (CTRL)
- 522 gRNA, 5 μg of psPAX2 and 1 μg of pMD2.G, using the standard calcium phosphate transfection
- 523 protocol.
- T98G cells were transduced with lentiviral particles and 72 hours post-transduction GFP-
- positive cells were sorted and pooled in a 6-well plate using a BD FACS melody. Cells were
- next amplified and IFNAR levels controlled by WB.

- 527 HEK293T^{DNA-PKcs-/-} clones and HEK293T^{CTRL} cells were generated by JetPrime (Polyplus)
- mediated transfection of LentiCRISPRv2GFP plasmid expressing the gRNA targeting the gene
- of interest or non-targeting control (CTRL) gRNA. Two days later GFP⁺ single-cell clones were
- selected on a BD FACSAria. Absence of DNA-PK expression was verified by WB.
- Primers for gRNA expressing constructs:
- 532 CTRL:
- 533 CACCGAGCACGTAATGTCCGTGGAT, AAACATCCACGGACATTACGTGCTC
- 534 IFNAR:
- 535 CACCGAGCTGACACTCACCTTCCCC, AAACGGGGAAGGTGAGTGTCAGCTC
- 536 PRKDC:
- 537 CACCGGCAGGAGACCTTGTCCGCTG, AAACCAGCGGACAAGGTCTCCTGCC
- 538 Cloning of DNA-PK expression vector:
- pcDNA3.1-nFlag-DNA-PK was cloned from synthesized gene fragments (eBlocks, IDT) based
- on consensus sequence ENST00000314191.7 modified for codon optimization. The gRNA
- 541 binding site targeted for knock-out was modified to prevent targeting by CRISPR/Cas9
- 542 constructs. N-terminal 3XFlag sequence including (GGGGS)₃ linker was added to the
- 543 synthesized template. pcDNA3.1 backbone was digested using BamHI and EcoRI,
- dephosphorylated using Quick CIP (NEB) and purified on agarose gel. eBlocks were amplified
- with KAPA HIFI HotStart Ready Mix (Roche) and purified on agarose gel. Gibson cloning was
- performed in two steps, with amplified and purified intermediate constructs, using NEBuilder
- 547 HiFi DNA Assembly Master Mix and NEB Stable Competent E. coli grown at 30°C. Resulting
- plasmid preparations were verified by whole plasmid sequencing.
- 549 Gene silencing
- 550 Silencing of DNA-PKcs was achieved in T98G cells using siRNAs and INTERFERin
- 551 (Polyplus) following the manufacturer's instructions. siRNAs (DharmaconTM; Horizon
- 552 Discovery) were used:
- 553 siCTRL: CGUACGCGGAAUACUUCGAUU
- 554 siDNA-PKcs: GAUCGCACCUUACUCUGUUUU
- 555 siKU70: ACAAGCAGUGGACCUGACUU
- 556 Cell treatment and transfection

- 557 Cells were plated in 6-well plate, or 100 mm dishes. Eighteen hours later, cells were pretreated
- with 2 μM NU7441 (#3712, Biotechne/Tocris) for 1 hour in DMEM or RPMI, prior to
- transfection with 2'3'-cGAMP (10 µg/ml, InvivoGen) using Lipofectamine 2000 (Thermo
- 560 Fischer Scientific), following the manufacturer's instructions. One, three or six hours after
- transfection, cells were harvested and stored at -80°C prior to 2'3'-cGAMP, protein or RNA
- 562 extraction.
- For other drug treatment, following 1 hour preincubation with Nu7441, cells were treated with
- 2'3'-GAM(PS)2 (Rp/Sp) (InvivoGen), or fluorinated 3'3'-cGAMP (InvivoGen) at 10 μg/ml,
- with diABZI compound 3 (InvivoGen) at 10 μM, with E7766 (MedChemExpress) at 1 μM, or
- 566 ADUS100 (MedChemExpress) at 50μM. Six hours later, cells were harvested and stored at
- 567 -80°C prior to protein or RNA extraction.
- 568 RNA extraction and gene expression analyses
- Total RNA was isolated with TRIzol (Invitrogen). RNA concentration was measured with a
- Nanodrop spectrophotometer (ND-1000, Nanodrop Technologies), prior to treatment with
- 571 TURBO DNase (Ambion) and cDNA synthesis from 1-2 μg RNA using SuperScript IV
- 572 (Invitrogen) using Oligo(dT) and quantification with a LightCycler 480 cycler (Roche) using
- 573 SYBR Green Master Mix (Takara) and appropriate primers. Relative quantities of the transcript
- were calculated using the $\Delta\Delta$ Ct method, using the Glyceraldehyde3-phosphate dehydrogenase
- 575 (GAPDH) for normalization, except for THP1 analyses were a normalization with
- 576 Hypoxanthine Phosphoribosyltransferase 1 (*HPRT1*) and Actin Beta (*ACTB*) was performed.
- 577 The RT-qPCR primers used are listed below:
- 578 GAPDH: For: CTGGCGTCTTCACCACCATGG, Rev: CATCACGCCACAGTTTCCCGG
- 579 ACTB: For: GGACTTCGAGCAAGAGATGG, Rev: AGCACTGTGTTGGCGTACAG
- 580 HPRT1: For: TGACACTGGCAAAACAATGCA, Rev: GGTCCTTTTCACCAGCAAGCT
- 581 IFNB1: For: GAATGGGAGGCTTGAATACTGCCT, Rev: TAGCAAAGATGTTCTGGA
- 582 GCATCTC
- 583 ISG15:For: GATCACCCAGAAGATCGGCG, Rev: GTTCGTCGCATTTGTCCACC
- 584 CXCL10: For: GAAAGCAGTTAGCAAGGAAAGGTG, Rev: ATGTAGGGAAGTGATG
- 585 GGAGAGG
- 586 IFIT1: For: GCCTTGCTGAAGTGTGGAGGAA, Rev: ATCCAGGCGATAGGCAGAGATC
- 587 IFIT2: For: GGAGCAGATTCTGAGGCTTTGC, Rev: GGATGAGGCTTCCAGACTCCAA

CCL5: For: CCTGCTGCTTTGCCTACATTGC, Rev: ACACACTTGGCGGTTCTTTCGG

588

618

Whole-cell lysate preparation and Western Blot 589 Cells were lysed in 5 packed cell volumes of TENTG-150 (20 mM Tris-HCl [pH 7.4], 0.5 mM 590 EDTA, 150 mM NaCl, 10 mM KCl, 0.5% Triton X-100, 1.5 mM MgCl2, and 10% glycerol, 591 supplemented with 10 mM β-mercaptoethanol, 0.5 mM PMSF and phosphatase inhibitor 592 (Sigma)) for 30 min at 4°C. Lysates were centrifuged 30 min at 14,000 g, and supernatants 593 were collected for WB. Protein quantification was performed using Bradford assay (Bio-Rad). 594 595 Protein samples were prepared in Laemmli buffer and heated at 95°C for 5 min prior to resolution by sodium dodecyl sulfate-polyacrylamide gel electrophoresis (SDS-PAGE) using 596 597 4-15% Mini-PROTEAN® TGXTM Precast Protein Gels (Bio-Rad). Proteins were transferred onto nitrocellulose membranes (Biorad Trans blot turbo). Proteins were visualized on 598 membranes using Ponceau S solution (Sigma-Aldrich) prior to 30 min blocking with (PBS) 599 containing 0.1% Tween (PBS-T) supplemented with 5% milk. Membranes were subsequently 600 incubated with primary antibodies in 5% milk/PBS-T (1:1,000 dilution, except when indicated) 601 for 2 hours at RT. Primary antibodies used include: anti-DNA-PKcs (A300-517, Bethyl, 1:500), 602 anti-cGAS (15102) Cell Signaling Technology), anti-pSTING Ser366 (19781, Cell Signaling 603 Technology), anti-STING (13647, Cell Signaling Technology), anti-pIRF3 Ser386 (ab76493, 604 Abcam), anti-IRF3 (11904, Cell Signaling Technology), anti-HSP90 (4877, Cell Signaling 605 Technology), anti-GAPDH (60004-1-Ig, Proteintech Europe, 1:5,000), αTUBULIN (66031-1-606 607 Ig, Proteintech Europe, 1:10,000). Membranes were incubated with Horseradish peroxidase (HRP)-coupled secondary antibodies (Cell Signaling Technology) at 1:2,000 dilution, for 1 608 hour at RT. Immunoreactivity was detected by Chemiluminescence (SuperSignal West Pico or 609 Femto, Thermo Fisher Scientific). Images were acquired on a ChemiDoc (Bio-Rad) or 610 Amersham Imager 680 (GE Healthcare). 611 612 Endogenous DNA-PKcs and FLAG-DNA-PKcs immunoprecipitation and assessment of interaction with 2'3'-cGAMP interaction 613 For immunoprecipitation of endogenous DNA-PKcs, T98G cells were lysed in 5 packed cell 614 volume of the lysis buffer 20 mM Tris-HCl [pH 7.4], 150 mM NaCl, 10 mM KCl, 0.5% Triton 615 X-100, 1.5 mM MgCl₂, and 10% glycerol, supplemented with 10 mM β-mercaptoethanol, 616 0.5 mM PMSF, for 30 min at 4°C on a wheel. Lysates were centrifuged 30 min at 14,000 g, 617

and supernatants were collected for immunoprecipitation. Endogenous immunoprecipitation

was performed using DNA-PKcs-targeting antibody (A300-517A, Bethyl), or Rabbit IgG

(Santa Cruz) as a negative control. After an overnight incubation at 4°C on a wheel,

immunoprecipitation was performed using Protein G Sepharose Fast Flow beads (Sigma). After

3 washes in lyses buffer, part of the bound material was either eluted in Laemmli buffer for WB

analyses, or used to assess DNA-PKcs:2'3'-cGAMP interaction.

624 FLAG-DNA-PKcs immunoprecipitation was performed by expressing FLAG-DNA-PKcs in

293T^{DNA-PKcs-/-} (C#2) for 48 hours prior to whole cell extract preparation as above and

immunoprecipitation using anti-FLAG dynabeads. Immunoprecipitates were analyzed by WB

or used to assess DNA-PKcs:2'3'-cGAMP interaction

620

621

622

623

625

626

627

631

632

633

634

635

636

637

638

639

640

641

642

643

644

645

646

647

648

649

To assess DNA-PKcs:2'3'-cGAMP interaction, bound material was incubated with an excess

of 2'3'-cGAMP diluted in lyses buffer, for 30 min on ice. After 3 washes with lyses buffer,

630 bound material was subjected to proteinase K treatment (15 min at room temperature) to

denature DNA-PKcs and allow the release of potential bound 2'3'-cGAMP. Proteinase K were

inactivated, incubating samples 10 min at 95°C, prior to measurement of 2'3'-cGAMP level by

enzyme-linked immunosorbent assay (ELISA).

Immunoprecipitation of Recombinant DNA-PKcs and assessment of interaction with CDN

For the immunoprecipitation of recombinant DNA-PKcs, 2 μg of anti-DNA-PKcs antibody or the corresponding IgG control was incubated with 70 ng of recombinant DNA-PKcs protein (Promega) in 500 μL of lysis buffer (20 mM Tris–HCl [pH 7.4], 150 mM NaCl, 10 mM KCl, 0.5% Triton X-100, 1.5 mM MgCl2, and 10% glycerol, supplemented with 10 mM β-mercaptoethanol, 0.5 mM PMSF). The mixture was incubated overnight at 4°C on a rotating wheel. The next day, the samples were centrifuged at 12,000 rpm for 10 min, and the supernatant was collected. Thirty μL of Sepharose beads (5 μL per immunoprecipitation point, for a total of 6 points) were added to the supernatant and incubated at 4°C for 45 min on a rotating wheel. Following incubation, the beads were centrifuged at 2,500 rpm and washed three times with the lysis buffer (without β-mercaptoethanol and PMSF). After washing, the immunoprecipitated complexes were incubated with the tested cyclic dinucleotides (CDNs), including 2'3'-cGAMP, 3'3'-cGAMP, and c-di-AMP, with or without NU7441. The incubation was performed with a CDN or nu7441 concentration 10 times higher than that of DNA-PKcs for 30 min on ice. After the incubation, the beads were washed, and the samples were digested

with proteinase K before measuring the amount of CDNs bound to DNA-PKcs by ELISA. 2'3'-

- 650 cGAMP, 3'3'-cGAMP and c-di-AMP ELISA were performed according to the manufacturer's
- protocol using the Cayman Chemical 2'3'-cGAMP ELISA Kit (CAY501700), 3'3'-cGAMP
- 652 ELISA Kit (CAY502130), c-di-AMP ELISA Kit (CAY501960), respectively.

Quantification of 2'3'cGAMP in T98G and 293T cells

- For intracellular 2'3'-cGAMP quantification, T98G or 293T cells were harvested 1 or 3 hours
- post 2'3'-cGAMP transfection, respectively, counted, washed in phosphate-buffered saline
- 656 (PBS) (Sigma), pelleted, and either directly processed or frozen at -80°C until extraction. 2'3'-
- 657 cGAMP extraction was performed using the commercially available Mammalian Protein
- Extraction Reagent (M-PER) buffer (Thermo Fisher), accordingly to the manufacture protocol.
- The recovered supernatants were used for 2'3'-cGAMP measurement, following adequate
- sample dilution. 2'3'-cGAMP amount in each sample was further normalized to the µg of
- proteins per sample.

662

ATP hydrolysis assay

- The ability of DNA-PK to hydrolyze ATP was measured by using the DNA-PK Kinase Enzyme
- 664 System coupled to the ADP-Glo Assay (Promega), following manufacturer's instructions.
- Briefly, 30 unit of human recombinant DNA-PK were incubated for 60 min at room temperature
- with 1 µM ATP, 1 x activator and 0.2 µg/µl substrate, in presence of increasing doses of 2'3'-
- 667 cGAMP (InvivoGen), 3'3'-cGAMP (InvivoGen), c-di-GMP (InvivoGen), c-di-AMP
- (InvivoGen), ADUS-100 (MedChemExpress), or E7766 (MedChemExpress). Incubation with
- 4 μM NU7441 was included as a positive control. After 1 hour, the reactions were incubated
- with 25 μL of ADP-Glo reagent for 40 min at room temperature, followed by incubation with
- 671 50 μL of Kinase Detection reagent for 30 min at room temperature. Luminescence was
- 672 measured using the FLUOstar Omega microplate reader (BMG Labtech).

673 Molecular Modelling Analyses

- 3D coordinates were obtained from the X-ray solved, Crystal Structure of Human DNA-
- dependent Protein Kinase Catalytic Subunit (DNA-PKcs) with RCSB code: 5LUQ. The full
- amino acid sequence for ATM, ATR and mouse DNA-PK were obtained from GenBank
- database. The sequence alignment was done using ClustalW. The alignment was repeated using
- 678 Hidden Markov Models yielding similar results as obtained by ClustalW, due to the
- conservation of several anchoring motifs throughout the alignment. Molecular docking studies

were executed using the ZDOCK suite, which relies on a three-dimensional fast Fourier transformation algorithm. ZDOCK uses a scoring function that returns electrostatic, hydrophobic and desolvation energies, and performs a fast pairwise-shape complementarity evaluation. Moreover, it uses the contact propensities of transient complexes to perform an evaluation of a pairwise atomic statistical potential for the docking molecular system.

RDOCK was utilized to refine and evaluate the results obtained by ZDOCK. RDOCK performs a fast energy minimization step to the ZDOCK molecular complex outputs and ranks them according to their re-calculated binding free energies. Energy minimizations were used to remove any residual geometrical strain in each molecular system, using the Amber99 force field as it is implemented into the Gromacs suite, version 4.5.5. All Gromacs-related simulations were performed through our previously developed graphical interface. An implicit Generalized Born (GB) solvation was chosen at this stage, to accelerate the energy minimization process. Subsequently, molecular systems were subjected to unrestrained Molecular Dynamics Simulations (MDS) using the Gromacs suite, version 4.5.5. MDS took place in a simple point charge (SPC) water-solvated, periodic environment. Water molecules were added using the truncated octahedron box extending 7Å from each atom. Molecular systems were neutralized with counter-ions as required. For the purposes of this study all MDS were performed using the NVT ensemble (i. e. constant Number of atoms, Volume and Temperature throughout the simulation) in a canonical environment, at 300 K and a step-size equal to 2 femto-seconds for a total 10 nanoseconds simulation time.

The quality and reliability of produced models in terms of 3D structural conformation was evaluated using the Gromacs package using a residue packing quality function, which depends on the number of buried non-polar side chain groups and on hydrogen bonding and the PROCHECK suite. Finally, the Molecular Operating Environment (MOE) suite was used to evaluate the 3D geometry of the models in terms of their Ramachandran plots, omega torsion profiles, phi/psi angles, planarity, C-beta torsion angles and rotamer strain energy profiles.

HSV-1 Infection

- 707 HSV-1-GFP and VSV-GFP infections, quantifications and imaging
- 708 The HSV-1 KOS-64-GFP strain (HSV-1-GFP) was a gift from S. R. Paludan (Aarhus
- university, Danemark). HSV-1 was amplified on Vero cells, aliquoted and frozen at -80°C.

- 710 Titration was performed on Vero cells, by serial dilutions and plaque formation assessment to
- 711 determine the multiplicity of infection (MOI).
- VSV-GFP was a gift from Dr Sebastien Pfeffer (IBMC, France). VSV-GFP was amplified on
- 713 BHK21 cells, aliquoted and frozen at -80°C. Single-round titration of the viral stock was
- performed on NIH-3T3 cells to determine the MOI.
- 715 2x104 T98G cells were seeded in 96 well plates in technical triplicates. The next morning, cells
- were pretreated or not for 1h with $2\mu M$ of NU7441. Cells were subsequently treated for 6h with
- either 10μM of diABZi, 1μM of E7766 or 10μg/ml of fluorinated 3'3'-cGAMP in the presence
- or not of 2μM NU7441. The cells were then infected with either HSV-1-GFP (for 1.5 h at MOI
- 719 2) or VSV-GFP (for 1 h at MOI 0.1) in DMEM without serum. Media was then replaced with
- either DMEM-10% FBS (VSV-GFP) or DMEM-1% human serum overnight and replaced with
- 721 DMEM-10% FBS the next morning (HSV-1-GFP). Cells were fixed with 4% PFA for 20 min
- either 16 h post-infection (for VSV-GFP) or 48 h post-infection (for HSV-1-GFP). Cells were
- 723 permeabilized with 0.2% Triton X-100 for 10 minutes at room temperature and nuclei were
- stained with DAPI.
- 725 The percentage of infected cells (i.e. GFP-positive cells) was quantified using an ImageXpress
- Pico (Molecular Devices) with a 4X lens. Values were averaged between technical triplicates.

727 Statistical analysis

- 728 Statistical analysis was performed using GraphPad Prism software. To compare data from two
- conditions, a standard unpaired two-tailed Student's t test was performed. One-way Anova with
- 730 Tukey's multiple comparisons test was used to analyze the ATP hydrolyses assay. The number
- of replicates in each experiment are indicated in the figure legends. All data are expressed as
- mean \pm SEM. Results were considered significant when p < 0.05. Ns: non-significant.
- 733 *P<0.05, **P<0.01, ***P<0.001 and ****P<0.0001

References

- Crowl, J. T., Gray, E. E., Pestal, K., Volkman, H. E. & Stetson, D. B. Intracellular Nucleic Acid Detection in Autoimmunity. *Annu Rev Immunol* **35**, 313-336, doi:10.1146/annurev-immunol-051116-052331 (2017).
- 739 2 Motwani, M., Pesiridis, S. & Fitzgerald, K. A. DNA sensing by the cGAS-STING pathway in health and disease. *Nat Rev Genet* **20**, 657-674, doi:10.1038/s41576-019-0151-1 (2019).
- Ablasser, A. & Chen, Z. J. cGAS in action: Expanding roles in immunity and inflammation. Science **363**, doi:10.1126/science.aat8657 (2019).
- 743 4 Sun, Z. & Hornung, V. cGAS-STING signaling. *Curr Biol* **32**, R730-R734, doi:10.1016/j.cub.2022.05.027 (2022).

- 745 5 Ou, L., Zhang, A., Cheng, Y. & Chen, Y. The cGAS-STING Pathway: A Promising Immunotherapy Target. *Front Immunol* **12**, 795048, doi:10.3389/fimmu.2021.795048 (2021).
- Decout, A., Katz, J. D., Venkatraman, S. & Ablasser, A. The cGAS-STING pathway as a therapeutic target in inflammatory diseases. *Nat Rev Immunol* 21, 548-569, doi:10.1038/s41577-021-00524-z (2021).
- 750 7 Sun, L., Wu, J., Du, F., Chen, X. & Chen, Z. J. Cyclic GMP-AMP synthase is a cytosolic DNA 751 sensor that activates the type I interferon pathway. *Science* **339**, 786-791, 752 doi:10.1126/science.1232458 (2013).
- Wu, J. *et al.* Cyclic GMP-AMP is an endogenous second messenger in innate immune signaling by cytosolic DNA. *Science* **339**, 826-830, doi:10.1126/science.1229963 (2013).
- Sun, W. *et al.* ERIS, an endoplasmic reticulum IFN stimulator, activates innate immune signaling through dimerization. *Proc Natl Acad Sci U S A* **106**, 8653-8658, doi:10.1073/pnas.0900850106 (2009).
- 758 10 Zhong, B. *et al.* The adaptor protein MITA links virus-sensing receptors to IRF3 transcription factor activation. *Immunity* **29**, 538-550, doi:10.1016/j.immuni.2008.09.003 (2008).
- 760 11 Hertzog, J. & Rehwinkel, J. Regulation and inhibition of the DNA sensor cGAS. *EMBO Rep* 21, e51345, doi:10.15252/embr.202051345 (2020).
- Vila, I. K., Guha, S., Kalucka, J., Olagnier, D. & Laguette, N. Alternative pathways driven by STING: From innate immunity to lipid metabolism. *Cytokine Growth Factor Rev* **68**, 54-68, doi:10.1016/j.cytogfr.2022.08.006 (2022).
- Hou, Y. et al. SMPDL3A is a cGAMP-degrading enzyme induced by LXR-mediated lipid metabolism to restrict cGAS-STING DNA sensing. *Immunity* **56**, 2492-2507 e2410, doi:10.1016/j.immuni.2023.10.001 (2023).
- 770 15 Mardjuki, R. *et al.* Identification of extracellular membrane protein ENPP3 as a major cGAMP hydrolase, cementing cGAMP's role as an immunotransmitter. *bioRxiv*, doi:10.1101/2024.01.12.575449 (2024).
- Jutte, B. B. *et al.* Intercellular cGAMP transmission induces innate immune activation and tissue inflammation in Trex1 deficiency. *iScience* **24**, 102833, doi:10.1016/j.isci.2021.102833 (2021).
- 775 17 McWhirter, S. M. *et al.* A host type I interferon response is induced by cytosolic sensing of the bacterial second messenger cyclic-di-GMP. *J Exp Med* **206**, 1899-1911, doi:10.1084/jem.20082874 (2009).
- Woodward, J. J., Iavarone, A. T. & Portnoy, D. A. c-di-AMP secreted by intracellular Listeria monocytogenes activates a host type I interferon response. *Science* **328**, 1703-1705, doi:10.1126/science.1189801 (2010).
- Burleigh, K. *et al.* Human DNA-PK activates a STING-independent DNA sensing pathway. *Sci Immunol* 5, doi:10.1126/sciimmunol.aba4219 (2020).
- Ferguson, B. J., Mansur, D. S., Peters, N. E., Ren, H. & Smith, G. L. DNA-PK is a DNA sensor for IRF-3-dependent innate immunity. *Elife* 1, e00047, doi:10.7554/eLife.00047 (2012).
- Hristova, D. B. *et al.* DNA-PKcs is required for cGAS/STING-dependent viral DNA sensing in human cells. *iScience* **27**, 108760, doi:10.1016/j.isci.2023.108760 (2024).
- Taffoni, C. *et al.* DNA damage repair kinase DNA-PK and cGAS synergize to induce cancerrelated inflammation in glioblastoma. *EMBO J* **42**, e111961, doi:10.15252/embj.2022111961 (2023).
- Sun, X. et al. DNA-PK deficiency potentiates cGAS-mediated antiviral innate immunity. Nat
 Commun 11, 6182, doi:10.1038/s41467-020-19941-0 (2020).
- Leahy, J. J. *et al.* Identification of a highly potent and selective DNA-dependent protein kinase (DNA-PK) inhibitor (NU7441) by screening of chromenone libraries. *Bioorg Med Chem Lett* **14**, 6083-6087, doi:10.1016/j.bmcl.2004.09.060 (2004).
- Paulis, A. & Tramontano, E. Unlocking STING as a Therapeutic Antiviral Strategy. *Int J Mol Sci* **24**, doi:10.3390/ijms24087448 (2023).
- 797 26 Yue, X., Bai, C., Xie, D., Ma, T. & Zhou, P. K. DNA-PKcs: A Multi-Faceted Player in DNA Damage Response. *Front Genet* **11**, 607428, doi:10.3389/fgene.2020.607428 (2020).

- Zhang, X. *et al.* Cyclic GMP-AMP containing mixed phosphodiester linkages is an endogenous high-affinity ligand for STING. *Mol Cell* **51**, 226-235, doi:10.1016/j.molcel.2013.05.022 (2013).
- 802 28 Burdette, D. L. *et al.* STING is a direct innate immune sensor of cyclic di-GMP. *Nature* **478**, 515-518, doi:10.1038/nature10429 (2011).
- Jin, L. *et al.* MPYS is required for IFN response factor 3 activation and type I IFN production in the response of cultured phagocytes to bacterial second messengers cyclic-di-AMP and cyclic-di-GMP. *J Immunol* **187**, 2595-2601, doi:10.4049/jimmunol.1100088 (2011).
- Perry, A. K., Chen, G., Zheng, D., Tang, H. & Cheng, G. The host type I interferon response to viral and bacterial infections. *Cell Res* **15**, 407-422, doi:10.1038/sj.cr.7290309 (2005).
- Lees-Miller, J. P. *et al.* Uncovering DNA-PKcs ancient phylogeny, unique sequence motifs and insights for human disease. *Prog Biophys Mol Biol* **163**, 87-108, doi:10.1016/j.pbiomolbio.2020.09.010 (2021).
- 812 32 Meek, K., Dang, V. & Lees-Miller, S. P. DNA-PK: the means to justify the ends? *Adv Immunol* **99**, 33-58, doi:10.1016/S0065-2776(08)00602-0 (2008).
- Blackford, A. N. & Jackson, S. P. ATM, ATR, and DNA-PK: The Trinity at the Heart of the DNA Damage Response. *Mol Cell* **66**, 801-817, doi:10.1016/j.molcel.2017.05.015 (2017).
- Harding, S. M. *et al.* Mitotic progression following DNA damage enables pattern recognition within micronuclei. *Nature* **548**, 466-470, doi:10.1038/nature23470 (2017).
- Taffoni, C. *et al.* Nucleic Acid Immunity and DNA Damage Response: New Friends and Old Foes. *Front Immunol* **12**, 660560, doi:10.3389/fimmu.2021.660560 (2021).
- Wu, J. *et al.* The multifaceted functions of DNA-PKcs: implications for the therapy of human diseases. *MedComm (2020)* **5**, e613, doi:10.1002/mco2.613 (2024).
- Hines, J. B., Kacew, A. J. & Sweis, R. F. The Development of STING Agonists and Emerging Results as a Cancer Immunotherapy. *Curr Oncol Rep* **25**, 189-199, doi:10.1007/s11912-023-01361-0 (2023).
- Yang, H., Yao, F., Marti, T. M., Schmid, R. A. & Peng, R. W. Beyond DNA Repair: DNA-PKcs in Tumor Metastasis, Metabolism and Immunity. *Cancers (Basel)* 12, doi:10.3390/cancers12113389 (2020).